AGU PUBLICATIONS

JGR

Journal of Geophysical Research: Space Physics

RESEARCH ARTICLE

10.1002/2017JA024460

Key Points:

- Near simultaneous penetration of undershielding and overshielding electric fields across different latitudes in the midnight sector
- Simultaneous suppression of equatorial plasma bubble in Indian region while occurrence of strong plasma bubbles over European sector
- Shorter periods (~70 min) of f_oF_2 are associated with PPEF, while larger periods of f_oF_2(>2 h) are associated with DDEF/winds and tides

Correspondence to:
S. Sripathi,
ssripathi.iig@gmail.com

Citation:
Singh, R., & Sripathi, S. (2017). Ionospheric response to 22–23 June 2015 storm as investigated using ground-based ionosondes and GPS receivers over India. *Journal of Geophysical Research: Space Physics*, *122*. https://doi.org/10.1002/2017JA024460

Received 12 JUN 2017
Accepted 10 OCT 2017
Accepted article online 16 OCT 2017

Ionospheric Response to 22–23 June 2015 Storm as Investigated Using Ground-Based Ionosondes and GPS Receivers Over India

Ram Singh[1] and S. Sripathi[1]

[1]Indian Institute of Geomagnetism, New Panvel, India

Abstract In this paper, we present response of equatorial and low-latitude ionosphere to 22/23 June 2015 geomagnetic storm using a chain of ground-based ionosondes located at Tirunelveli (8.73°N,77.70°E; geomagnetic latitude: 0.32°N), Hyderabad (17.36°N, 78.47°E; geomagnetic latitude: 8.76°N), and Allahabad (25.45°N, 81.85°E; geomagnetic latitude: 16.5°N) along with a chain of GPS receivers. Uniqueness of this storm is that in contrast to the equatorial plasma bubbles that were detected in the European sector, we see suppression of plasma bubbles in the Indian sector. The observations suggest that westward penetration electric field during local midnight caused abrupt decrease of virtual height ($h'F$ (km)) to ~200 km and suppressed plasma bubbles due to undershielding. Later, the layer increased to 500 km simultaneously due to overshielding effect. On 23 June, we observed negative storm in the Northern Hemisphere while positive storm in the Southern Hemisphere. In addition, absence of equatorial E_s layers at Tirunelveli and presence of F_3 layer at Tirunelveli/Hyderabad seem to be associated with equatorial electrojet (EEJ)/counter electrojet (CEJ) variations. However, on 24 June, we observed strong negative storm effects at Allahabad/Hyderabad, while positive storm effect at Tirunelveli. Simultaneous enhancement of $h'F$ (km) at all three ionosonde stations at 20:30 UT on 23 June during recovery phase suggest eastward disturbance dynamo (DD) electric field that caused presunrise spread *F* at Hyderabad/Allahabad but void of spread *F* at Tirunelveli suggesting its midlatitude origin. Periodogram analysis of f_oF_2 and $h'F$ (km) in the present analysis suggest the presence of shorter periods (~< 2 h) associated with prompt penetration (PP) electric fields while larger periods (>2 h) associated with DD electric field/winds.

Plain Language Summary The observations suggest near simultaneous penetration of undershielding and overshielding electric fields across different latitudes in the midnight sector along Indian longitude. There is simultaneous suppression of equatorial plasma bubble in Indian region while strong plasma bubbles over European sector at the same time. Results indicate that shorter period (<70 min) oscillations are associated with prompt penetration electric fields, while larger periods (>2 h) are associated with disturbance dynamo electric fields or disturbance winds and tides.

1. Introduction

Interplanetary and solar wind conditions play significant role in understanding the coupling between high- and low-latitude ionospheres during geomagnetic storms. It is essential to know the conditions of the interplanetary electric fields/magnetic fields to understand the storm time electrodynamics over equatorial and low latitudes. It is known that satellites get damaged during such major space weather events by the impinging solar wind particles. Several satellites such as Advanced Composition Explorer (ACE) have been launched to study the coupling between solar wind and Earth's magnetosphere (e.g., Astafyeva et al., 2016; Cassak, 2016; Hapgood, 2017; Liu et al., 2014; Ramsingh et al., 2015; Verkhoglyadova et al., 2016). These satellites provide unique opportunity to understand the coupling nature between solar wind-magnetosphere-ionosphere system where the solar wind, magnetosphere, and ionosphere from a single system driven by the transfer of energy and momentum from the solar wind to magnetosphere-ionosphere (e.g., Kamide et al., 1997, 1998; Somayajulu, 1998; Tsurutani & Gonzalez, 1997; Wolf, 1975).

During geomagnetic storm, the sudden southward/northward turning of the interplanetary magnetic field (IMF) B_z produces a dawn to dusk convection electric fields often known as prompt penetration electric fields (PPEFs) at high latitude resulting in an undershielding or overshielding condition depending upon the polarity of the IMF B_z (e.g., Fejer et al., 1979; Gonzales et al., 1979; Kikuchi et al., 2003, 2000; Rastogi & Patel, 1975).

These electric fields transmitted almost instantly to the equatorial regions through a transverse magnetic mode propagating in the Earth ionosphere waveguide (e.g., Kikuchi, 1986). The region 1 (R1) and region 2 (R2) field-aligned currents and their horizontal closure currents play an important role in generating these global scale ionospheric electric fields. These currents respond directly to solar wind conditions such as the orientation and magnitude of IMF B_z, solar wind velocity, and dynamic pressure (e.g., Kelly et al., 1979; Kikuchi et al., 1996). The northward turning of IMF B_z resulting in an overshielding electric field during the recovery phase of magnetic storm (e.g., Huang et al., 2005; Kikuchi et al., 2008). Eastward/westward electric field perturbations during daytime/nighttime are associated with sudden increase in the convection electric field. The direction of PPEF during daytime will be in eastward to the dusk sector and during the nighttime it will be in a westward direction to the dawn sector (e.g., Fejer et al., 1990; Jaggi & Wolf, 1973). These electric field perturbations usually have smaller amplitudes and shorter lifetime compared to the disturbance electric fields associated with substorm activity. These electric fields are most common near dusk and in the early morning-noon period (e.g., Kikuchi et al., 1996; Sastri et al., 1992). Several investigations have been made to estimate the penetration efficiency of these PPEFs over equator (e.g., Huang et al., 2007; Kelley et al., 2003). It is believed that PPEFs mostly penetrate with efficiency of 10% (Huang et al., 2007). However, these efficiencies are highly local time dependent and are larger on the nightside than on the dayside.

The electric field in the equatorial ionosphere during geomagnetic storms is manifested by the two physical processes, namely, (a) solar wind magnetospheric dynamo, associated with prompt penetration of the magnetospheric convection electric fields (PPEFs) (e.g., Sastri et al., 1997; Spiro et al., 1988), and (b) the ionospheric disturbance dynamo electric fields (DDEFs) and disturbed winds, associated with the global thermospheric wind circulation that is caused due to Joule heating at high latitudes (e.g., Araki et al., 1985; Blanc & Richmond, 1980; Kikuchi, 1986). When the IMF B_z polarity turns southward direction, undershielding electric field promptly penetrate to the equatorial latitudes with eastward polarity in the sunset sector causes enhancement in the Pre-Reversal Enhancement (PRE) vertical drift that could lead to the instability growth rate and equatorial spread F (ESF) generation. It is believed that longitudinal conductivity gradient in the ionosphere during sunset sector causes enhanced vertical plasma drifts and produces super fountain effect (sometimes) and plasma bubbles that can reach very high latitudes (e.g., Basu et al., 2001). However, when the IMF B_z suddenly turns northward, overshielding westward electric fields leads to the suppression of both PRE and ESF (e.g., Fejer et al., 1981; Abdu et al., 1981; Fejer et al., 1990; Sastri et al., 2000). Liu et al. (2014) studied the combined effects of PPEF and DDEF over the East Asian/Australian sector. Also, they have suggested that the multiple PPEF can occur when the IMF B_z is in stable southward direction. The other type of disturbances also couples to the equatorial and low-latitude ionosphere and produces variations; however, these disturbances propagate to equator with a time delay of above 3 h (e.g., Blanc & Richmond, 1980; Fejer et al., 1983; Sastri, 1988).

The disturbed electric fields and neutral winds can disturb the equatorial plasma density and plasma transport through equatorward contraction/poleward expansion of the equatorial ionization anomaly (EIA) crest due to changes in the ionospheric heights (increase or decrease in the height of the F_2 layer through meridional winds). Simultaneously, the photo ionization and neutral compositions will change at equatorial and low latitudes according to the strength of the auroral activity which is known as positive (increase in f_oF_2)/negative (decrease in f_oF_2) ionospheric storm effects (e.g., Basu et al., 2001; Batista et al., 2006; Heelis & Coley, 2007; Lei et al., 2008; Liu et al., 2014; Mannucci et al., 2005; Tsurutani et al., 2004). Blanc and Richmond (1980) reported that the zonal component of disturbance dynamo electric field is westward during the day and eastward during the nighttime, which is opposite to the daytime/nighttime ionospheric dynamo electric fields. The observations of equatorial electrojet (EEJ), F region plasma drifts and electron densities during geomagnetic storm indicate that the DDEFs can significantly affect the low-latitude ionosphere (e.g., Fejer et al., 1983; Sastri, 1988, 1989). During the storm period, DDEF can cause the suppression of equatorial ionization anomaly (EIA) and also cause the negative ionospheric storm, that is, reduction of total electron content (TEC) during the daytime (e.g., Tsurutani et al., 2004), while during nighttime with eastward polarity of DDEF can enhance the F layer height, which is the result of intensification of EIA (Abdu, 1997). There are instances where both disturbance dynamo and prompt penetration electric fields coexisted and simultaneously operated in the ionosphere such as 15 July 2000 storm (e.g., Basu et al., 2001; Sastri et al., 2002).

The atmospheric gravity waves (AGWs) or traveling ionospheric disturbances (TIDs) generated due to enhanced Joule heating in the auroral latitudes during geomagnetic storms also play a crucial role in causing positive/negative storms at low-middle latitudes through reduction of [O]/[N_2] ratio trough the transport of ionized particles to lower latitudes with an increase in the temperature and N_2 density (e.g., Lee et al., 2002; Liu et al., 2014; Mikhailov & Schlegel, 1998; Richmond & Matsushita, 1975). Due to large differences in the energy deposition rates at high latitudes over Northern Hemisphere/Southern Hemisphere, significant compositional change exists in the Northern and Southern Hemispheres. A three-dimensional, time-dependent model of the coupled thermosphere and ionosphere is utilized to explain the preference for negative storms in summer and positive storms in winter by Fuller-Rowell et al. (1996). The model results suggest that the prevailing summer-to-winter circulation at solstice transports the molecule-rich gas to middle and low latitudes in the summer hemisphere in a day or two following the storm. In the winter hemisphere, poleward winds restrict the equatorward movement of composition. The altered neutral-chemical environment in summer subsequently depletes the *F* region midlatitude ionosphere to produce a negative storm, while in winter midlatitudes a decrease in molecular species, associated with downwelling, persists and produces the characteristic positive storm.

In this paper, we present an interesting piece of observation during 22/23 June 2015 space weather event where we observed westward penetration of electric fields during midnight sector in the Indian sector, while eastward penetration was dominant over European sector. While westward penetration in the midnight sector is reported by Sastri et al. (2002) over Indian sector due to *AE* index, we report here both eastward and westward penetration electric fields associated with orientation of IMF B_z. Uniqueness of this storm is that in contrast to the equatorial plasma bubbles that were detected at midlatitudes in the European sector due to strong upward plasma drifts as shown by Cherniak and Zakharenkova (2016), we observed suppression of plasma bubbles due to downward drifts in the Indian sector. Astafyeva et al. (2016) have studied the ionospheric response to this storm using SWARM satellites. Their observations indicated that dayside ionosphere experienced a strong negative ionospheric storm effect, while on the nightside an extreme enhancement of the topside TEC occurred at midlatitudes of the Northern Hemisphere. The dayside ionosphere responded to the occurrence of the strong eastward equatorial electric fields and then penetration of westward electric fields led to gradual but strong decrease of the plasma density on the dayside in the topside ionosphere. On the nightside, they suggested that extreme enhancement of the density and TEC in the Northern Hemisphere in the topside ionosphere are related to the combination of the prompt penetration electric fields, disturbance dynamo, and the storm time thermospheric circulation. Based on our observations, we are trying to understand the electrodynamic response of the equatorial and low-latitude ionosphere over Indian sector in the wake of these recent observations. Also, since this storm falls in solstice period, it would also give us an opportunity to know the impact of varied background conditions on the storm time variations in the ionospheric parameters and compare these results with that of equinox storms such as March 2015 St. Patrick's Day geomagnetic storm.

2. Data Sets

The results presented in this paper are obtained from a chain of ionosondes and GPS receivers located in Indian sector for 22/23 June 2015 geomagnetic storm event. The solar wind parameters are from the CDAWEB (http://cdaweb.gsfc.nasa.gov), and these data are obtained from the ACE satellite measurements. The geomagnetic activity indices like *Kp*, *AE*, and *SYM-H* are obtained from the WDC (World Data Center). The ionospheric parameters, namely, *h′F* and foF2, are scaled manually using data obtained from three Canadian Advanced Digital Ionosondes (CADI) operating at an equatorial station, Tirunelveli (TIR) (8.73°N, 77.70°E; geomagnetic latitude: 0.34°N), Hyderabad (HYD) (17.36°N, 78.47°E; geomagnetic latitude: 8.76°N), a low-latitude station and Allahabad (ALD) (25.3°N, 81.5°E; geomagnetic latitude: 16.5°N), which is located in the northern edge of the equatorial ionization anomaly (EIA) crest region. The ionograms at TIR and HYD are obtained at 10 min interval, while we collected ionograms at ALD at every 5 min interval. We collected 1 min TEC data from the GPS receiver (Scintillation Network Decision Aid (SCINDA)) at Tirunelveli, Global Navigation Satellite System (GNSS) receivers at Mumbai (19.09°N, 73.11°E), and Nagpur (21.14°N, 79.08°E; geomagnetic latitude: 12.42°N), and 5 min interval GPS TEC data provided by MIT Haystack Observatory Madrigal database (http://madrigal.haystack.mit.edu/madrigal/). The strength EEJ, which is the difference of ΔH_{TIR} and ΔH_{ABG} ($\Delta H_{TIR} - \Delta H_{ABG}$), as measured by the two pairs of ground-based magnetometers,

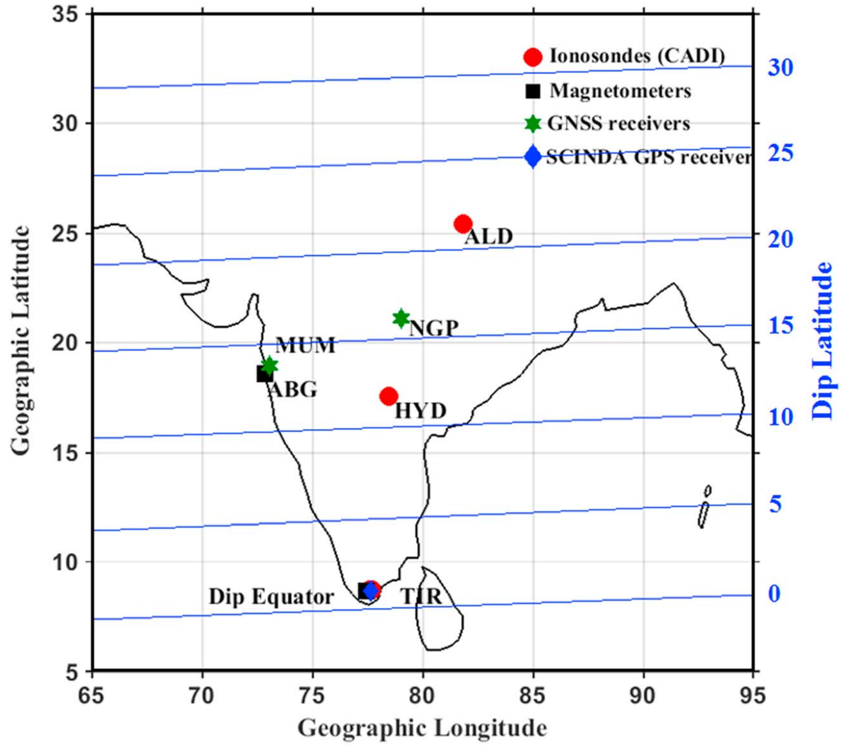

Figure 1. Shows the location of various stations and instruments used in the present study.

namely, Tirunelveli (H_{TIR}) (8.73°N, 77.70°E), an equatorial station, and Alibag (H_{ABG}) (18.5°N, 72.9°E), an off-equatorial station, is also utilized. Figure 1 shows the location of various stations used in the present paper, and Table 1 shows the list of stations along with their instruments as used in the present study.

3. Results

3.1. Interplanetary Conditions on Geomagnetic Storm of 22/23 June 2015

The magnetic storm of 22/23 June was the second largest geomagnetic storm event after the St. Patrick's Day (17 March 2015) geomagnetic storm event in the current solar cycle-24. The main cause of this storm event was two coronal mass ejections (CMEs) that hit the Earth's magnetopause at 05:45 UT and at 18:35 UT on 22 June 2015, and geomagnetic field activity ranged from quiet to severe storm conditions. This summer solstice storm event in 2015 is selected for the special VarSITI data analysis. Figures 2a–2d show the time-corrected 1 min variations of the near-Earth solar wind parameters from the ACE satellite (in GSM coordinates) at the L1 point, namely, solar wind pressure (P_{sw}), solar wind velocity (V_{sw}), IMF B_z, and interplanetary electric field (IEF_y) during 22–24 June 2015. At the 22/05:45 UT, a small shock was observed at the ACE spacecraft. During the shock time IMF B_z reached from ~6 nT (northward) to ~−10 nT (southward) (Figure 2c) with a corresponding solar wind speed increase from 350 km/s to 430 km/s (Figure 2b), the pressure reached up to 10 nPa (Figure 2a). At 22/18:30 UT, another shock was observed with significant changes in the interplanetary

Table 1
Shows the List of Stations Which We Used in Our Study

Station	Instruments	Geographic latitude	Geographic longitude	Geomagneticlatitude
Tirunelveli (TIR)	CADI, Magnetometer and SCINDA GPS receiver	8.73°N	77.7°E	0.34°N
Hyderabad (HYD)	CADI	17.36°N	78.47°E	8.76°N
Alibag (ABG)	Magnetometer	18.5 °N	72.9°E	10.36°N
Mumbai (MUM)	GNSS receiver	19.09°N	73.11°E	10.37°N
Nagpur (NGP)	GNSS receiver	21.14°N	79.08°E	12.42°N
Allahabad (ALD)	CADI	25.43°N	81.84°E	16.48°N

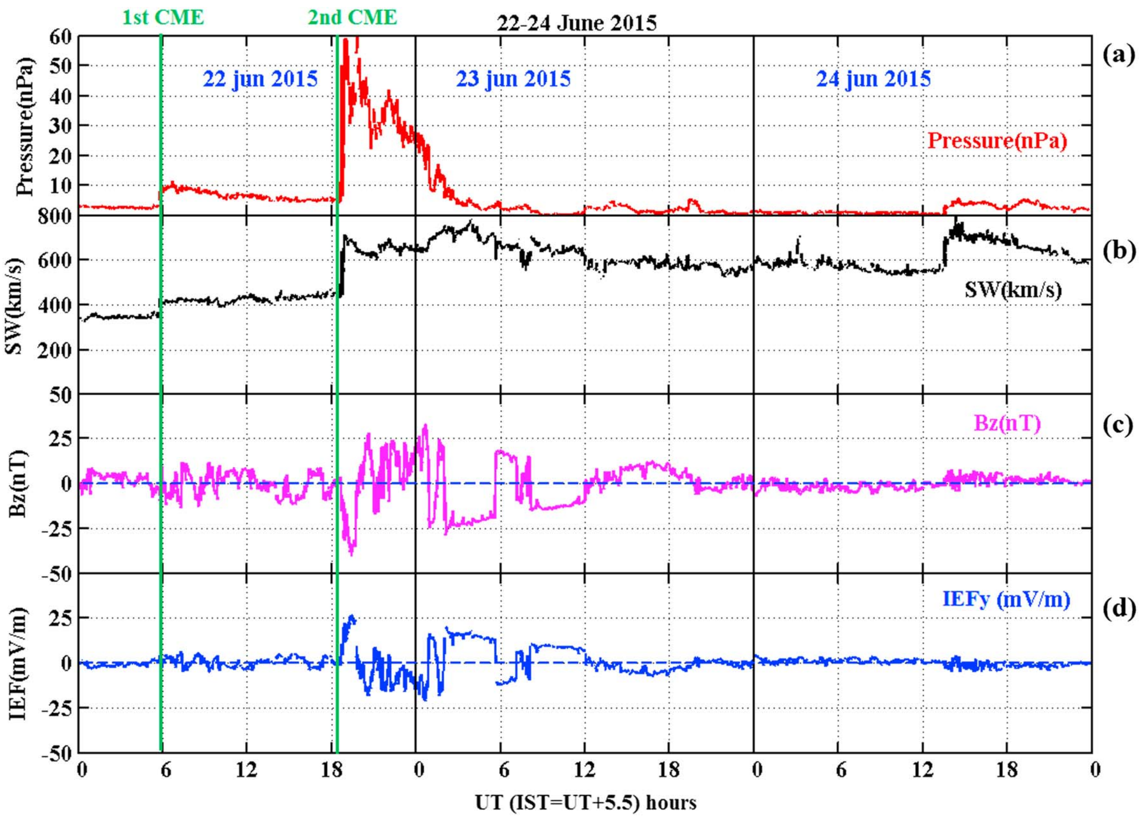

Figure 2. Solar wind parameter's variation (a) solar wind pressure, (b) solar wind velocity, (c) interplanetary magnetic field (IMF B_z), and (d) interplanetary electric field (IEF), during 22–24 June 2015.

parameters due to the arrival of second CME. The P_{sw} reached from ~5 to ~60 nPa (Figure 2a), V_{sw} suddenly increased from ~440 to ~720 km/s (Figure 2b), and IMF B_z component suddenly turned southward with its minimum value of ~−40 nT at 22/19:30 UT in undershielding condition. After, the IMF B_z went northward up to ~28 nT nearly at 22/20:30 which represents the overshielding condition; again, IMF B_z slowly went back to southward and reached ~−17 nT, fluctuating between ±25 nT around 3–4 h, 22/21:00 to 22/23:59 UT. After that, the IMF B_z sharply turned northward to southward and reached ~−25 nT at ~23/00:30 UT and suddenly back to northward. However, after, the IMF B_z continued for some time in the southward direction with a magnitude of ~−20 nT around 23/02:00 to 23/05:00 UT. It again slowly turned northward for some time ~ 3 h with magnitude of ~16 nT; after that, it went southward and slowly turned southward to northward on 23 June. When the IMF B_z was southward same time IEF reached up to ~25 mV/m on 22/19:30 (Figure 2d).

Now the impact of the above solar wind parameters is investigated through observations in the ground magnetic field observations in the next plot. Figures 3a–3d are showing the auroral electrojet (*AE*) index, *SYM-H*, equatorial electrojet (EEJ) strength, and *Kp* index during 22–24 June. It may be noted that while the first shock of CME did not show any changes on 22 June, however, the second shock of CME impacted the high and middle latitudes where auroral electrojet (*AE*) index jumped from ~500 nT to ~2,300 nT (Figure 3a) and positive disturbance in *SYM-H* index (Figure 3b) reached up to ~88 nT due to the enhanced of Chapman Ferraro currents in magnetopause. During this period, the *Kp* index was initially in the range of 5 which went up to 8 (Figure 3d) and *SYM-H* initially reached its first minimum value of ~−133 nT on 22/20:30 UT, and after that it reached its minimum value of ~−207 nT on 23/04:30 (Figure 3b). This was followed by the onset multiple substorms as can be seen in *AE* index. During the main phase of the storm, a decrease in the *H* component of the geomagnetic field is seen in *SYM-H* component implying the ring current intensification. In the recovery phase which is characterized by increase in the H component shows the normal behavior on 23–24 June. From the Figure 3c, EEJ strength showed the eastward electric fields (EEJ) and westward electric fields (CEJ) on 22 June around 06:00 to 12:00 UT. However, on 23 June, initially, the EEJ strength was ~50 nT up

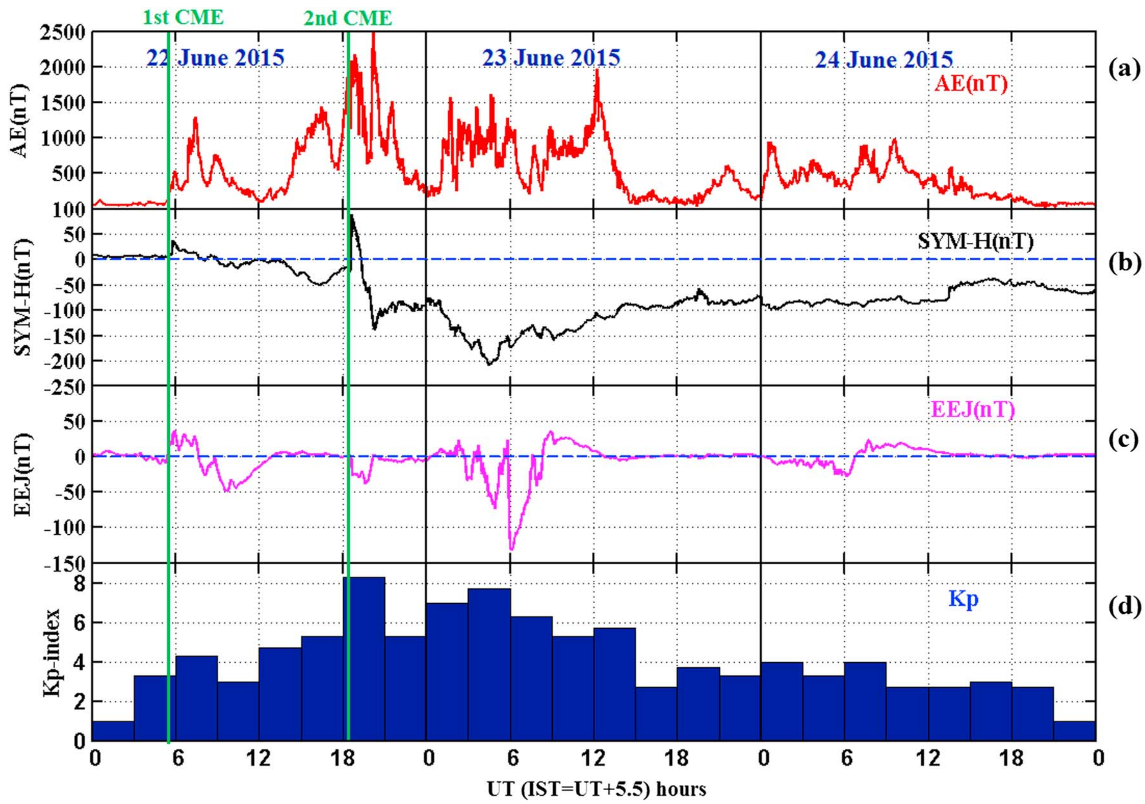

Figure 3. The variation of (a) auroral electrojet (*AE*) index, (b) *SYM-H*, (c) EEJ strength, and (d) *Kp* index for the period of 22–24 June 2015.

to 02:30 UT; after that, EEJ reached ~−50 nT (CEJ) and again turned to the positive value of ~50 nT. However, a strong CEJ with its value of ~−145 nT is observed during ~06:00 UT. On the 24 June 2015, the CEJ is observed around 06:00 UT. It is suggested that low-latitude electric fields can get enhanced/reduced since the convection electric field enhances/drops suddenly associating with the IMF B_z turning southward/northward. Rastogi and Patel (1975) suggested that CEJ at the equator can be due to the reversal of penetrating electric fields. Similarly, EEJ strength can undergo strong fluctuations due to disturbance dynamo effect during geomagnetic storms.

3.2. Latitude Variation of the Ionosphere as Seen by Chain of Ionosondes

In the previous figure, we explained about interplanetary and auroral activity conditions during June 2015 storm. Next, we will present its response in the equatorial and low-latitude ionosphere in Figures 4a–4e. The figure gives a general overview of the latitude variation of the *F* region ionosphere during 22–24 June 2015. Here we are showing the impact of different phases of the magnetic storm on the low-latitude ionosphere. We will highlight some important results in this work. Figures 4a–4c show the variation of *F* region virtual height (*h′F*) over Tirunelveli (equatorial), Hyderabad (low latitude), and Allahabad (low-latitude, EIA northern crest region), respectively, while Figures 4d and 4e show the IMF B_z and EEJ strength variations during 22–24 June 2015. It may be mentioned that the local time is 5 h 30 min ahead of UT. In Figures 4b and 4c, green color lines indicate the F_3 layers observed at Tirunelveli and Hyderabad stations on 22–24 June. We also plotted the mean and its standard deviation of virtual height in Figures 4a–4c during five International Quiet Days (IQDs) in June 2015 which is shown in blue curve. In the same figure, the black bold line indicates spread *F* durations. The black curve in Figure 4e shows the five IQD mean variations of EEJ. During June 2015, the five IQDs are 02, 03, 04, 05, and 20. It may be noted that the data gaps in *h′F* over all three stations are due to the bad ionogram traces. From the figure, it can be seen on 22 June that initially *h′F* shows normal behavior over all three stations, while IMF B_z varies its values between ±10 nT, and EEJ is showing EEJ/ CEJ signatures with its value of ~−50 nT between 06:00 UT (11:30 LT) and 12:00 UT (17:30 LT). The first CME influence is not seen in the figures.

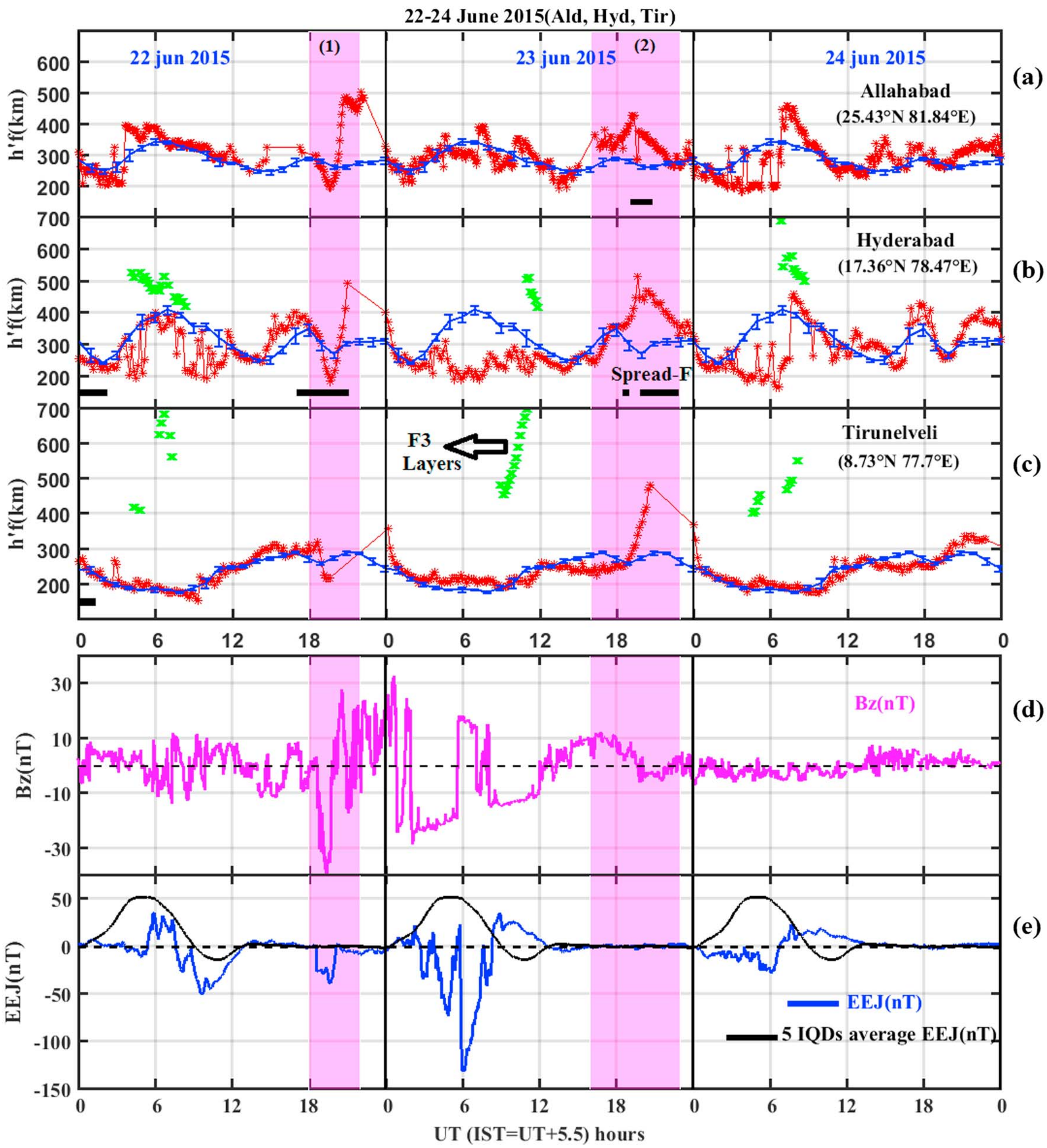

Figure 4. Temporal variation of ionospheric F region parameters (a) $h'F$ in kilometers (red), and five IQDs mean value (blue) of $h'F$ at ALD; (b) $h'F$ in kilometers (red), and five IQDs mean value (blue) of $h'F$ at HYD; (c) $h'F$ in kilometers (red) and five IQDs mean value (blue) of $h'F$ at TIR; (d) IMF B_z; and (e) EEJ strength (blue), and five IQDs mean value (black) of EEJ; bold black lines indicate spread F, and green color lines indicate the F_3 layers (Figures 4b and 4c) over Indian region, during 22–24 June 2015.

However, the 2nd CME that hits the Earth's magnetopause at 18:30 UT on 22 June initiates geomagnetic storm and its main phase occurs at 19:00 UT (00:30 LT). At the same time, $h'F$ (virtual height) simultaneous sharply started decreasing and reached its minimum value over all three stations that coincide with sudden southward turning of IMF B_z and CEJ in Figure 4 (shaded region (1)). Immediately, sudden jump in $h'F$ is noticed over all three stations when B_z returned northward at 21:30 UT (03:00 LT) on 22 June.

During this period, auroral activity (AE) showed its maximum value of ~2,500 nT at 20:30 UT (02:00 LT) as can be seen in Figure 3. This AE intensification suggests the strong prompt penetration of auroral electric field to low latitudes due to the substorm activity during the storm time on 22 June. The reductions in $h'F$ (~19:00 UT (00:30 LT) could be due to the southward turning of IMF B_z with the westward PPEF and enhancements in $h'F$

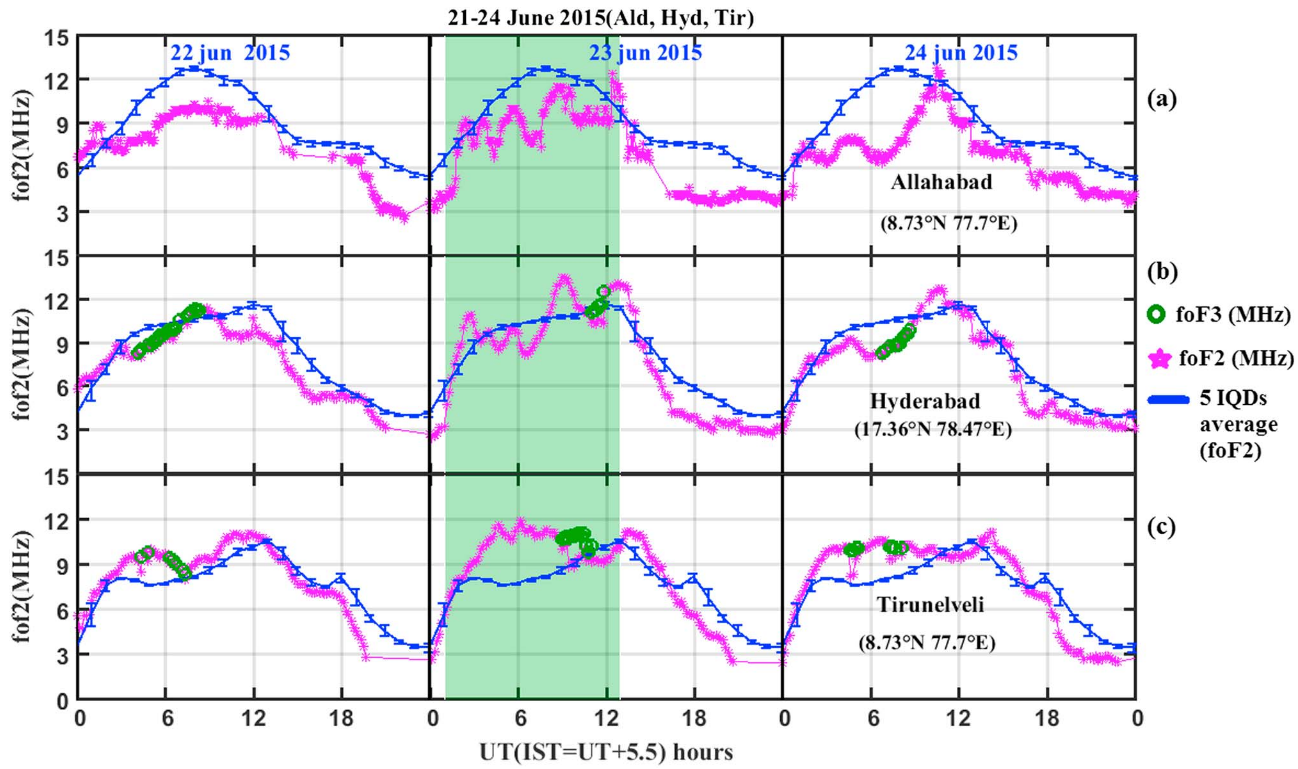

Figure 5. The temporal variations in (a) f_oF_2 (magenta) and five IQDs mean (blue) of f_oF_2 at ALD, (b) f_oF_2 (magenta) and five IQDs mean (blue) of f_oF_2 at HYD, (c) f_oF_2 (magenta) and five IQDs mean (blue) of f_oF_2 at TIR and green color circles indicate foF3 (critical frequency of F_3 layer) during the 22–24 June 2015.

(~21:30 UT (03:00 LT)) due to the northward turning of IMF B_z with the PP eastward electric field, where this westward/eastward PPEF will reduce/enhance the zonal electric field giving to the downward and upward $E \times B$ drifts. On 23 June, in the second shaded region in the figure, *h′F* is showing a significant enhancement compared to their quiet day average value during the recovery phase over all three stations where the *h′F* reached its maximum value of ~500 km at TIR, ~510 km at HYD, and ~460 km at ALD at 20:30 UT (02:00 LT), which could be due to the eastward disturbance dynamo electric field. On the 24 June, virtual height (*h′F*) at Tirunelveli showing the normal behavior and does not reflect any storm effect. However, at HYD and ALD stations, *h′F* height showed variation of tidal ion layer structures which are slowly descending with time. Such structures are more common at these stations during summer period. The tidal ion layers are believed to be generated by the tidal winds through the wind shear mechanism. Though these layers could also be impacted by geomagnetic storms, however, we have not investigated this aspect in this paper.

3.3. Spread *F* or Plasma Density Irregularities and f_oF_2 Variations

Here we discuss about salient features of ionospheric density variations from all three stations. Figures 5a–5c show the f_oF_2 (critical frequency of F_2 layer) variations at three equatorial and low-latitude stations during 22–24 June 2015 over Indian region. Here the blue curve with scatter bars indicate the five IQDs mean variation of f_oF_2 at respective stations and green color circles represent the critical frequency of F_3 (f_oF_3 (MHz)) layers over the equatorial and low-latitude stations. As can be seen, on the 22 June, the f_oF_2 value increases at ~02:30–13:00 UT (08:00–18:30 LT) in the equatorial station at TIR, while its value decreases at ~03:00–07:00 UT (08:30–12:30 LT) in HYD and at ~02:30–13:00 UT (08:00–18:30) in ALD compared to their quiet days mean value. On 23 June, f_oF_2 values significantly increased at two stations over TIR (~02:30–11:30 UT (08:00–17:00 LT) and HYD (02:30–03:30) and 09:30–14:30 UT (08:00–09:00 LT)) but at the ALD f_oF_2 values decreased ~02:30–14:00 UT (08:00–19:30 LT). On the 24 June, there is a significant reduction in f_oF_2 where it reduced its minimum value to 6 MHz with respect to its quite time average value at ~03:10–09:40 UT (08:40–15:10 UT) over ALD and HYD ~03:50–09:00 UT (09:20–14:30 UT). After the

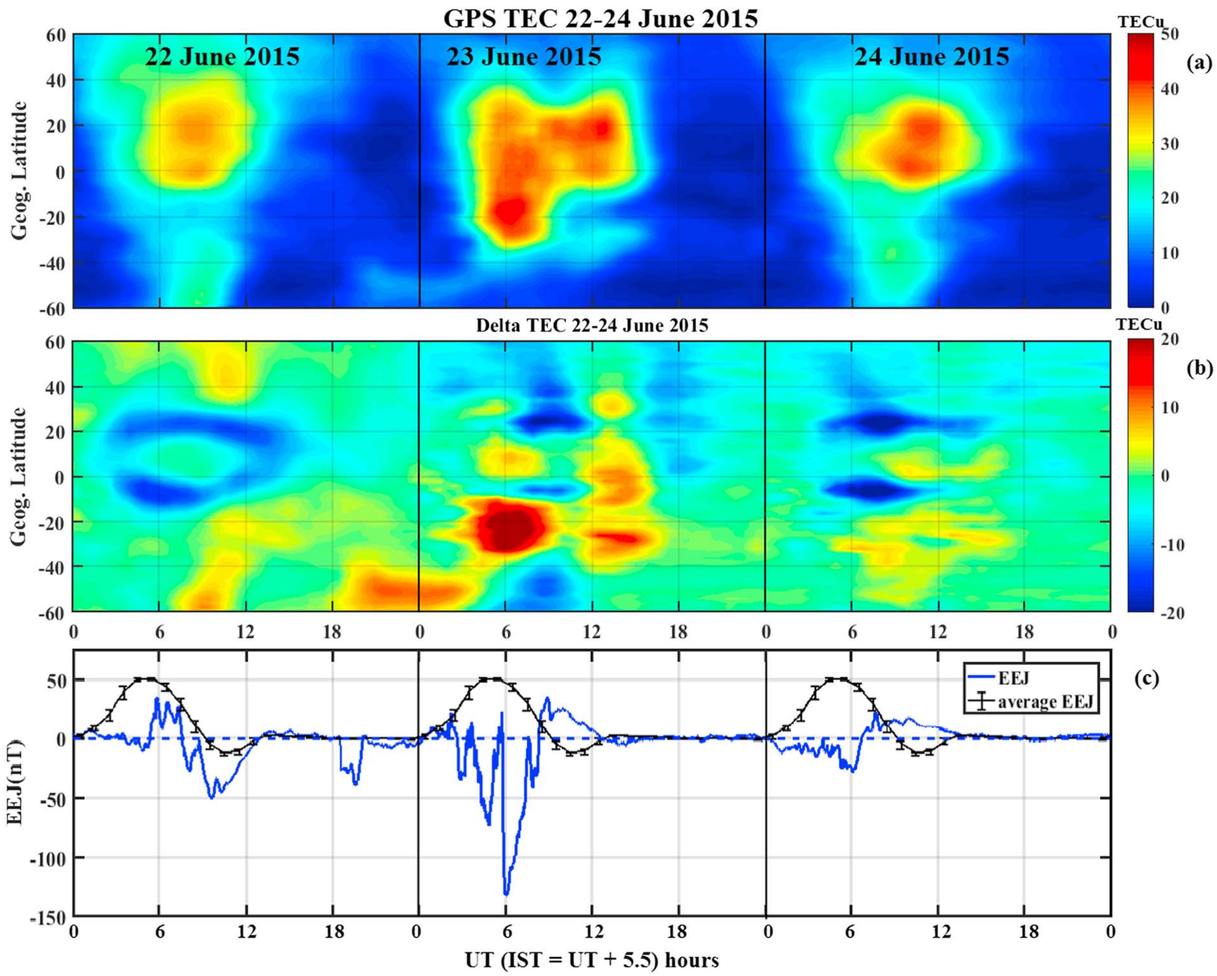

Figure 6. The (a) latitudinal and temporal variation of TEC (contour map); (b) ΔTEC = (TEC − TEC_{IQDsM}); TEC_{IQDsM} is the five IQDs mean variation during the June month, over 80°E longitude using GPS TEC data provided by MIT Haystack Observatory Madrigal database; (c) EEJ strength (blue) and five IQDs mean value (black).

decrement in f_oF_2 sudden increment over both stations reach its maximum value ~12 MHz, while over the TIR during this period no such kind of decrement in f_oF_2 is noticed. This enhancement and decrement in f_oF_2 shows the positive and negative ionospheric storm effects which are related to electric field disturbances. On the 22 June, the spread *F* was present at ~00:00–02:00 UT (05:30–08:00 LT) at TIR/HYD but spread *F* is seen at ~16:00–21:30 UT (21:30–03:00 LT) only at HYD station. However, on 23 June, the spread F is observed only at the low-latitude stations at Allahabad ~19:10–21:50 UT (00:40–03:20 LT) and Hyderabad ~18:50–22:50 UT (00:20–04:20 LT) but not at Tirunelveli.

3.4. Latitudinal Variation of GPS TEC During 22–23 June 2015

To investigate the temporal and latitudinal variation of TEC, we investigated the TEC variations using GPS TEC maps during this storm period. Figures 6a–6c show the temporal and latitudinal variation of TEC, ΔTEC, and EEJ strength, respectively, during 22–24 June 2015. Here ΔTEC = (TEC − TEC_{IQDsM}) are the absolute difference of TEC from the reference of five International Quiet Days mean value (TEC_{IQDsM}). As can be seen in the Figure 6, the equatorial ionization anomaly (EIA) significantly suppressed, two crest of EIA were absent on 22–24 June. On the 22 June, EIA is suppressed and partially shifted to the Northern Hemisphere up to 0°–35° geographic latitude at ~05:30–11:30 UT (11:00–17:00 LT). This suppression of EIA/absent of crest formation/ negative ionospheric storm effect is due the westward electric field on this day, which we can see clearly in the Figure 5c that EEJ is showing strong westward electric field (CEJ). In Figure 6b, the ΔTEC shows a significance enhancement in the Northern and Southern Hemispheres. The ΔTEC enhancement in the Southern Hemisphere is higher than the Northern Hemisphere between ~03:00 and 12:00 UT

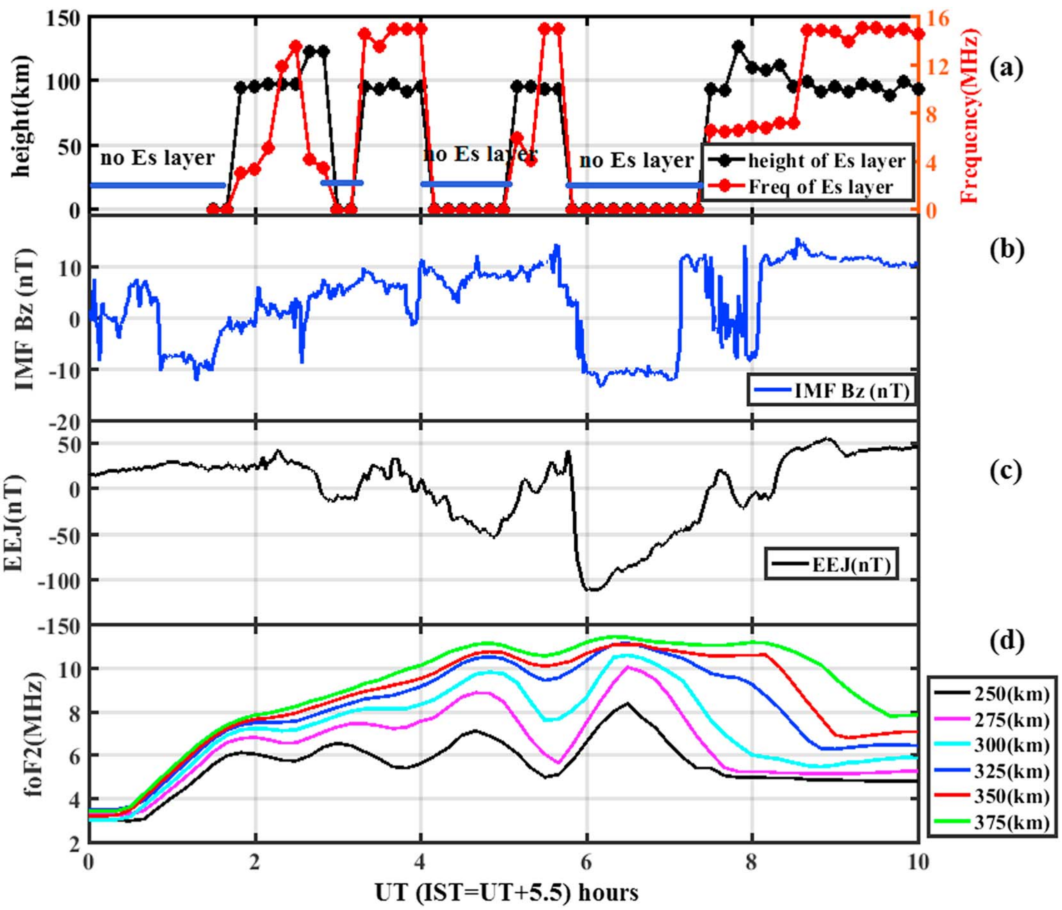

Figure 7. The (a) virtual height ($h'E_s$ (km)) of E_s layer (black); frequency of E_s layer (f_oE_s (MHz)). Blue color lines indicate the disappearance of E_s layer duration. (b) Variation of IMF (B_Z). (c) EEJ strength variations. (d) Isoheight variation over Tirunelveli, during the 23 June.

(08:30–17:30 LT), while the ΔTEC value is higher in Northern Hemisphere between ~13:00 and 16:00 UT (18:30–22:00 LT) on 23 June. This enhancement and suppression in the TEC values are similar to multiple counter electrojet (CEJ) occurring on this day. During the daytime on 24 June, EEJ has a minimum value of ~−40 nT at 06:00 UT (11:30 LT); after that, the EEJ went up to ~30 nT. This westward EEJ is mostly observed due to the DDEFs. The suppression of EIA and negative ionospheric storm in the Northern Hemisphere on the 24 June is due to the strong westward DDEFs.

3.5. Disappearance of E_{sq} Layer and Its Relation to EEJ and Isofrequency Variations

As seen in the earlier figures, temporal variation of EEJ strength during main phase of the storm fluctuates between positive/negative strength in association with prompt penetration of high-latitude electric fields. These fluctuations are believed to be associated with south/northward orientations of the IMF B_z activity. It is observed that equatorial q type E_s layers are suppressed whenever disturbed time/quiet time CEJ events are dominant over equator. In order to study the association of E_{sq} linked with storm time CEJ events, we analyzed temporal variation of E_{sq} layers over TIR which is shown in Figures 7a–7d. In the figure, we plotted the temporal variation of (a) virtual height ($h'E_s$ (km)) of E_s layer (black), frequency of E_s layer (f_oE_s (MHz)), (b) IMF B_z, (c) EEJ strength, and (d) isoheight variation at 250–375 km over Tirunelveli during the 23 June. The observations indicate that there was disappearance of E_{sq} layers whenever CEJ occurrence is observed. Also, isoheight variations show variations similar to EEJ/CEJ fluctuations. This suggests that there is a good correlation between CEJ occurrence and absence of E_{sq} and altitude variation of F layer over Tirunelveli.

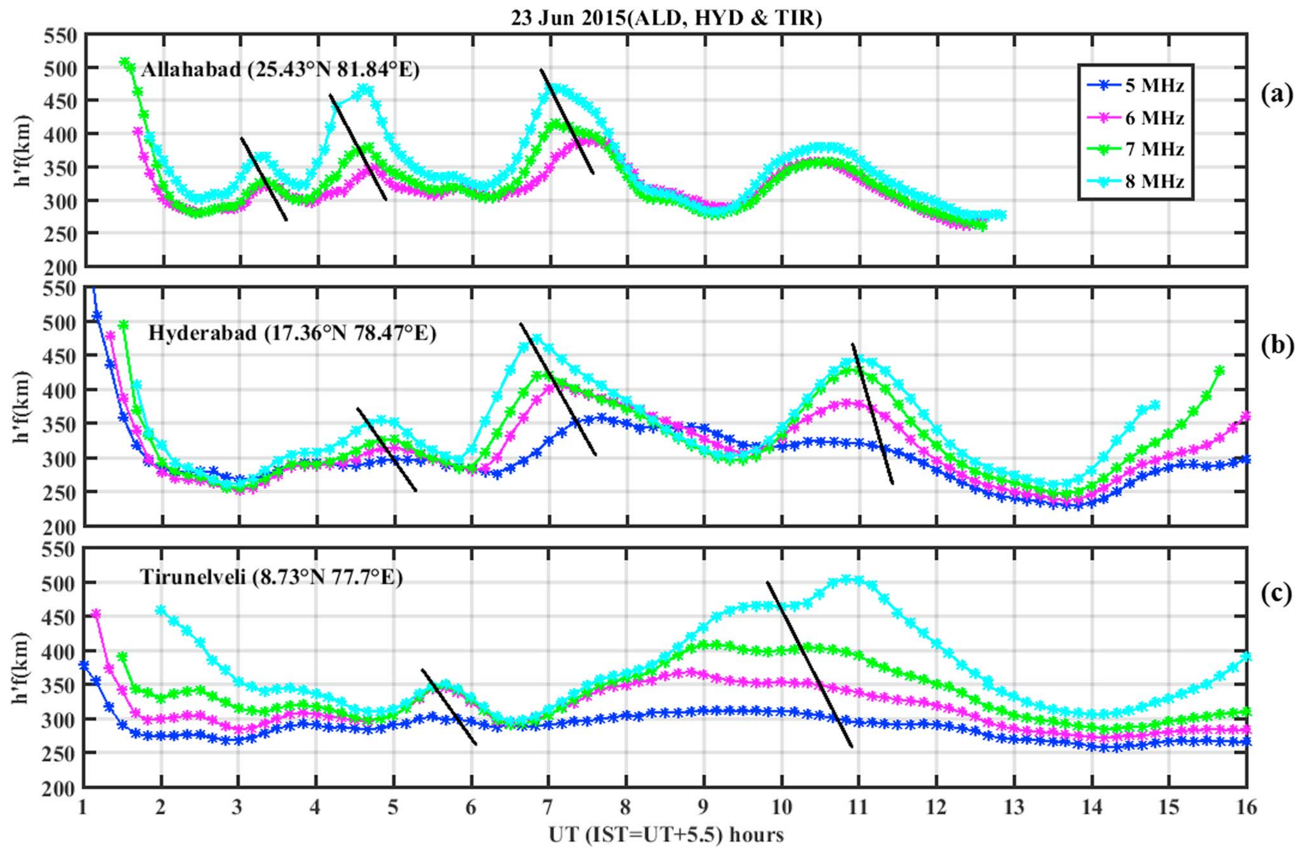

Figure 8. The temporal variation of isodensity plot at (a) Allahabad (6–8 MHz), (b) Hyderabad (5–8 MHz), and (c) Tirunelveli (5–8 MHz) stations. The black lines indicate phase velocity.

3.6. Traveling Ionospheric Disturbances in the f_oF_2, $h'F$ (km), and TEC

It is known that Joule heating is generated when auroral currents flow along the longitudinal conductivity gradients during intense geomagnetic storm activity. Due to this Joule heating, traveling ionospheric disturbances (TIDs) and equatorward meridional winds that propagate to equator are produced. In order to study the TID signatures during the present storm, we plotted the ionosonde height variations at four frequencies, namely, 5, 6, 7, and 8 MHz as obtained from all three stations in Figures 8a–8c. To better understand the oscillatory characteristics at different stations, isoheight analysis between 250 and 375 km heights with a 25 km range resolution at all three stations are also plotted in Figures 9a–9c. From the figures, it may be noticed that we are observing first density peak in Figure 8 at low-latitude station at Allahabad and the same variations are seen after ~1.5 h delay over Hyderabad and 2.5 h delay at Tirunelveli. The horizontal phase propagation of traveling ionospheric disturbances (TIDs) as calculated from the time delays is works out to be ~200 m/s from Allahabad to Hyderabad and ~300 m/s from Hyderabad to Tirunelveli based on the distances between Allahabad, Hyderabad, and Tirunelveli, respectively. As also can be seen from previous Figure 5 through shaded region in green that the f_oF_2 shows the oscillatory behavior in their temporal variation over all three stations between ~02:30 and 13:30 UT (08:00–19:00 LT) on 23 June similar to Figures 8 and 9. These oscillatory disturbances in electron density are due to the role of meridional neutral winds and traveling ionospheric disturbances (TIDs) from the high-latitude disturbances toward the equator. During the magnetic storm time due to the high auroral activity and joule heating, it is possible that the TIDs could have propagated to low latitude from high latitude.

Figures 10a–10c show the diurnal variation of vertical TEC variations over Nagpur, Mumbai, and Tirunelveli stations during 23 June 2015. Here the different colors indicate different PRN (Pseudo-Random Number) numbers. Elevation threshold of 30° is applied while plotting these TEC values. From the figure, it can be noticed that while TEC values sharply increases to 40 TEC units at 04:00 UT after sunrise in the morning at

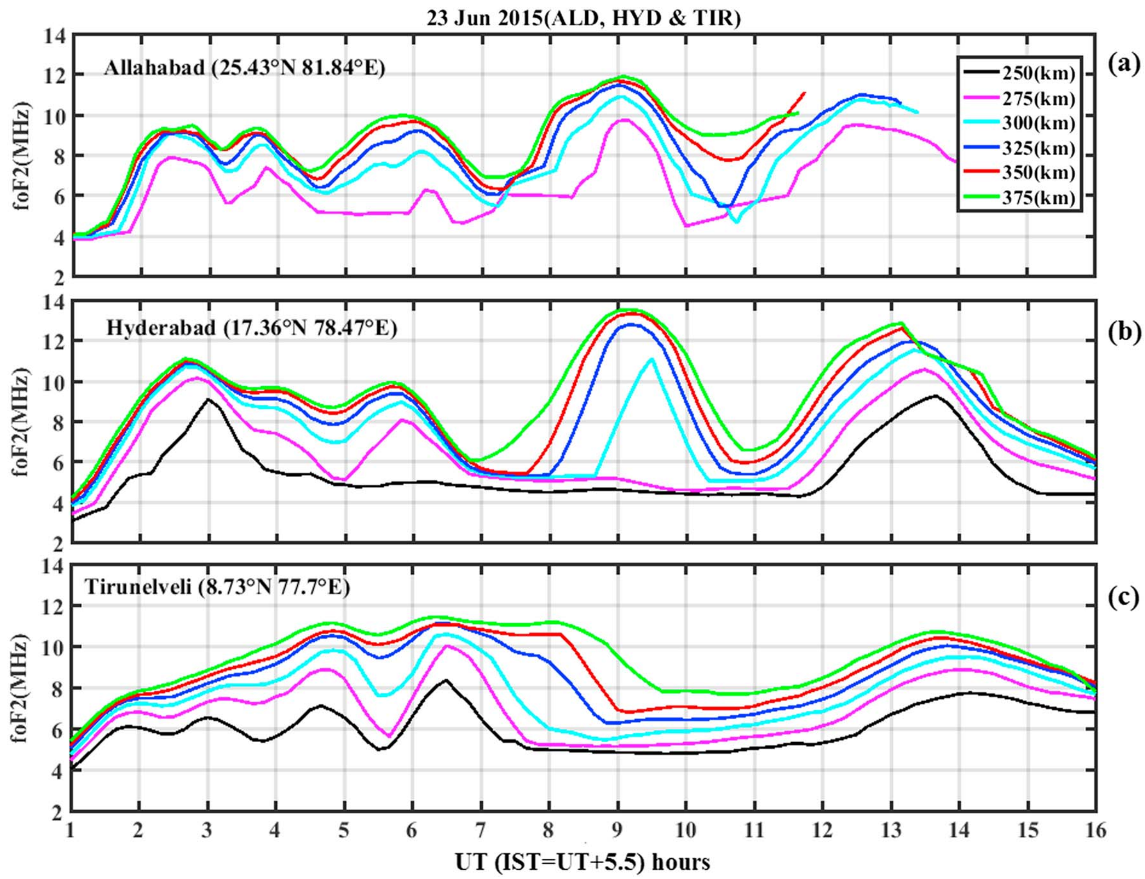

Figure 9. The variation of isoheight (km) plot at (a) Allahabad (275–375 km), (b) Hyderabad (250–375 km), and (c) Tirunelveli (250–375 km) stations.

Tirunelveli than over Nagpur/Mumbai stations at similar times. After that, TEC values are more like plateau at Tirunelveli with some fluctuations in TEC up to 14:00 UT. However, TEC values slowly increases in the morning at Hyderabad/Allahabad and they appear to be linearly varied with time up to 12:00 UT. However, there exists large-scale wave-like fluctuations in TEC in both Mumbai and Nagpur stations, however, with some phase delay between these stations. The observations suggest that these delays appear to be related to TIDs as noticed in ionosonde observations. After 12:00 UT, TEC is increased very much over Nagpur and Mumbai station than that of TIR station. After 14:00 UT, TEC sharply fell down to 10–15 TEC units over Tirunelveli than Mumbai/Nagpur stations. Based on these observations, we can suggest that clearly TIDs do propagated to low latitudes on 23 June as can be seen in the Figures 6–9 with some time delay between ~02:30 and 13:30 UT (08:00 19:00 LT).

3.7. Periodogram Analysis of Solar Wind/Ionospheric Parameters

It is always difficult to delineate variations of electric field, waves, and neutral wind signatures without performing periodogram analysis. To identify different periods and their sources, we performed periodogram analysis on the data. Figures 11a–11f shows the variation of IMF B_z, *AE* index, and EEJ strength and their fast Fourier transform analysis (periodogram) during 07:00 to 14:00 IST (Indian standard time) on the 23 June. Similarly, Figures 12a and 12b shows the f_oF_2 variations at TIR/HYD/ALD and their periodogram analysis during 07:00–14:00 IST. In Figures 11 and 12, blue color circles indicate the dominant periods which are the same in IMF B_z, *AE*, EEJ, and f_oF_2. It is clear from the figure that the dominant periods in IMF B_z are ~40, 70, and 90 min; in EEJ are ~40, 70, and 110 min; and in *AE* index are ~40, 70, and 140 min. In the Figure 12, the dominant periods are ~70, 90, and 160 min. Here we can see that the multiple periodicities and some common significant periodicities ($<$ 70 min) are present in all parameters (IMF B_z, *AE*, EEJ, and f_oF_2). From the Figures 11 and 12, we can notice that the IMF B_z, *AE* index, f_oF_2, and EEJ show the periodic oscillations at ($<$70 min) periods (in blue circle) and larger periods ($>$2 h). Periodogram analysis of equatorial and low-

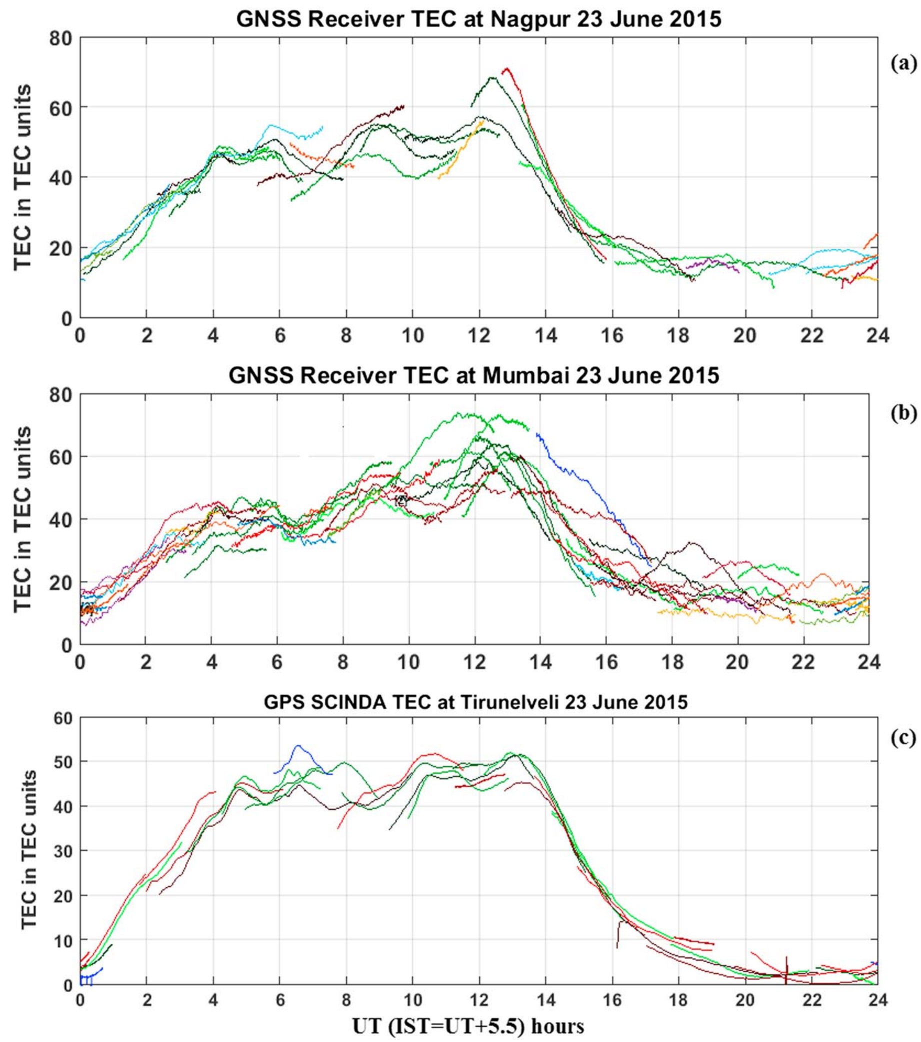

Figure 10. The variations of GPS TEC over Indian stations (a) Nagpur, (b) Mumbai, and (c) Tirunelveli during 23 March 2015.

latitude ionospheric data suggest that the shorter periods (~70 min) are found to be associated with IMF B_z variations while larger periods (> 2 h) are found to be associated with the high-latitude auroral activity. Some of the observed periods are well correlated with the auroral variations and ionospheric parameters (f_oF_2 and EEJ) of similar periods, which indicate the ionospheric effects are associated with some channel of energy penetration from the interplanetary space and magnetosphere.

4. Discussions

The important points that emerge from the previous section can be summarized as follows: (1) the strong PPEF penetrate simultaneously right from the equator to low latitudes with reduction/enhancement in the virtual height simultaneously over ALD, HYD, and TIR due to the penetration of westward/eastward electric fields in the undershielding and overshielding conditions; (2) strong F_3 layer occurrence during storm main phase; (3) suppression of midnight spread *F* during westward penetration in contrast to European sector; (4) traveling ionospheric disturbances (TID) signatures which are seen initially at low latitudes as propagated from midlatitudes possibly associated with high-latitude auroral activity and appears to be propagating to the equator; (5) appearance/disappearance of E_{sq} layers at Tirunelveli in association with storm time EEJ/CEJ variations; (6) negative/positive storm effects in the TEC; (7) pre-sunrise spread *F* observations at low-latitude stations, namely, Hyderabad and Allahabad but absence of spread *F* at equatorial station,

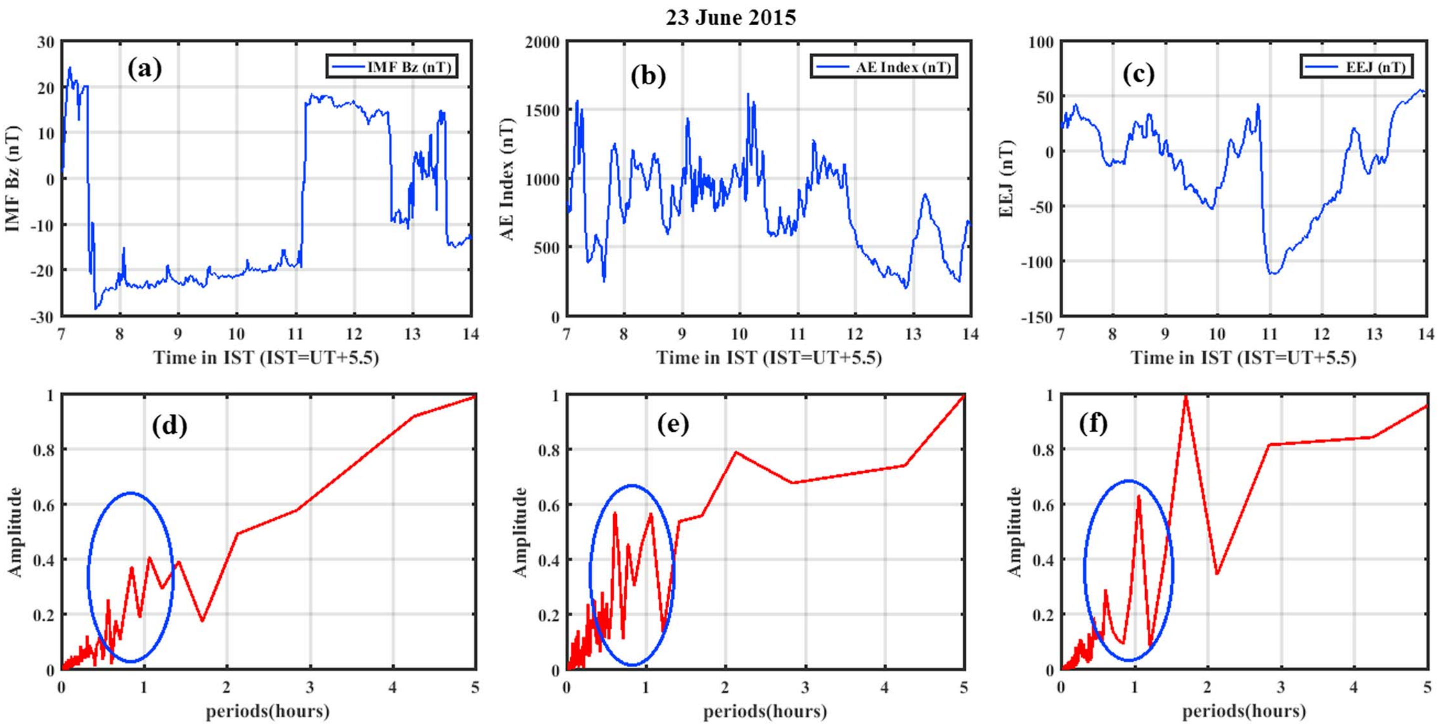

Figure 11. The B_z, *AE*, and EEJ variations and their periodogram (a) interplanetary magnetic field (B_z), (b) *AE*, (c) EEJ, (d) periodogram of B_z (red), (e) *AE* index (black), and (f) EEJ strength (red) and blue color circles indicate the dominant periods during the 23June 2015.

namely, Tirunelveli; (8) periodogram analysis of EEJ strength and electron density structures indicating existence of distinct (a) short-period ($<$ 70 min) and (b) long-period ($>$ 2 h) oscillations.

In order to understand these results and their relation to earlier storms, we have to understand storm time equatorial dynamics. It is known that significant compositional and electrodynamical changes occur in the equatorial and low-latitude ionosphere during disturbed periods due to changes in the thermosphere-ionosphere brought in by the disturbed thermospheric neutral winds and high-latitude Joule heating. The prompt penetration electric field occurs in the low-latitude region during the sudden southward (undershielding electric field) or northward (overshielding electric field) turning of the interplanetary magnetic field (IMF B_z) (Abdu et al., 1998, Fejer et al., 1995; Kikuchi et al., 1996; Sastri et al., 1992). The observations of reduction and enhancement in virtual height in the midnight sector on the 22 June 2015 over several Indian stations is believed to be due to undershielding and overshielding convection electric field. An earlier report by Ramsingh et al. (2015) showed the eastward PPEFs during evening sector on St. Patrick's Day geomagnetic storm where it is observed that strong upward vertical drift of ~70 m/s produced large TEC gradients, strong ionospheric scintillations, and plasma bubbles over wide latitudes over Indian region. In addition, large equatorward surge of meridional winds and zonal westward drifts is noticed in their observations. However, the results presented in this paper are in contrast to St. Patrick's Day storm where we see suppression of plasma bubbles over Indian sector. Since our drift data are contaminated by noise due to non–spread *F* event, we were unable to examine the zonal drift direction and its magnitude. On the other hand, Cherniak and Zakharenkova (2016) have reported intense plasma bubble of equatorial origin reaching to midlatitudes in the European sector in the dusk sector for the 22–23 June storm

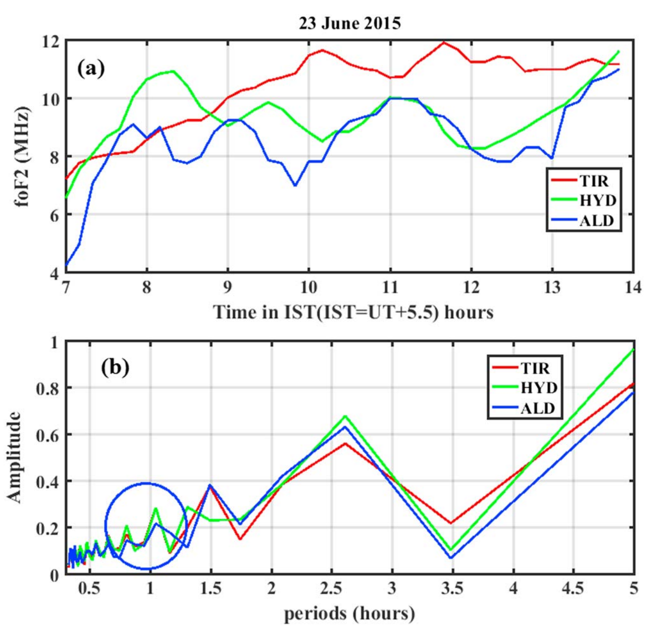

Figure 12. (a) The variation of f_oF_2 over Tirunelveli (red), Hyderabad (green), and Allahabad (blue); (b) periodogram of f_oF_2 of Tirunelveli (red), Hyderabad (green), and Allahabad (blue); blue color circle indicates the dominant periods during the 23June 2015.

using several GPS receivers in association with SWARM satellites. They suggested that their results of equatorial type plasma bubbles observed at midlatitudes possibly due to eastward penetration of electric fields on 22 June storm and caused strong upward drift such that the plasma bubbles map to midlatitudes. Theoretically, it is possible that equatorial plasma bubbles can reach to midlatitudes through super fountain effect; we believe that this is for the first time such report is made available through observations. However, we observed suppression of *F* layer height to ~200 km altitude sharply. This suggests that there exists a strong longitudinal variation in this storm. Since this storm is observed during June solstice where usually weak vertical drifts prevails, downward drift of *F* layer over equator to this storm is not significant as compared to 15 July 2000 storm where downward drift of ~215 km/h is noticed by Sastri et al. (2002). However, since plasma drifts are seen in the midlatitudes over European longitude during this storm, the vertical drifts during PRE could have been enhanced to several orders with reference to quiet time drifts. Sastri et al. (2000) have shown drastic reduction of *F* layer height simultaneously at several Indian stations at midnight period for the 15 July 2000 storm and suggested that reduction of *F* layer height is associated with westward penetration under eastward DD electric fields. They suggested that the westward penetration is associated with impulsive ring current injections. On the other hand, Basu et al. (2001) have shown that eastward penetration of electric fields in association with IMF B_z turning southward over South Atlantic region using ROCSAT satellite along with scintillations and TEC observations for the same geomagnetic storm. For this storm, initially, since AE index was very high (~1000 nT), the disturbance dynamo caused westward drifts in the evening sector, but due to IMF B_z turning southward in the midnight sector over South Atlantic, it produced strong upward drifts and caused strong VHF/L band scintillations.

Study of storm time disturbance dynamo electric field effects at equator by Blanc and Richmond (1980) have indicated that disturbance dynamo electric fields will be eastward during nighttime, while they are westward during daytime. In fact, Basu et al. (2001) showed that disturbance dynamo impacted first during the storm and later the prompt penetration of high-latitude electric fields when the disturbance dynamo effect was alive in the dusk sector. Though 22–23 June storm is not as strong as that of 15 July 2000 storm in terms of *Dst* index, however, many interesting similarities have been noticed. During this storm also, initially, *AE* index reached to ~1,000 nT due to first CME arrival. So intense auroral activity might have generated disturbance dynamo electric fields and winds which might have impacted the equatorial latitudes in a similar way as that of 15 July 2000 storm. Keskinen et al. (2003) have studied the evolution of equatorial ionospheric bubbles during a large increase of auroral electrojet (*AE*) index in the recovery phase. They have found that the storm time plasma bubble evolution is different from that of quiet time. Based on SAMI2 model and observations, they suggested that reduction of *E* region conductivity increases the storm time vertical drift that distinguishes the large *AE* increase during recovery phase of the storm time. Since we observed downward drift in our observations, it is possible that *E* region conductivity might have enhanced.

It is known that enhancement in the f_oF_2 as compared to that of quiet time variation is considered as positive storm, while decrease of f_oF_2 is considered as negative storm. Several authors have investigated the case studies of positive and negative ionospheric storm effects by taking the topside and bottomside ionosphere using the GPS-TEC and ground-based ionosondes (e.g., Zhao et al., 2012). In addition, there exists a preference for negative storms in summer hemisphere and positive storms in winter hemisphere. Fuller-Rowell et al. (1996) explained this preferential positive/negative storms in summer/winter hemisphere using a three-dimensional time-dependent model of the coupled thermosphere and ionosphere. Their results suggest that prevailing summer-to-winter circulation transports the molecule-rich gas to middle and low latitudes in the summer hemisphere in a day or two following the storm at solstice. However, in the winter hemisphere, poleward winds restrict the equatorward movement of composition. The altered neutral-chemical environment in summer subsequently depletes the *F* region midlatitude ionosphere to produce a negative storm, while in winter midlatitudes a decrease in molecular species, associated with downwelling, persists and produces the characteristic positive storm. Kil and Paxton (2006) have studied the global TEC maps during 15 July 2000 storm which also falls in June solstice as our storm and suggested that seasonal effects can be characterized by negative ionospheric storm (decrease in plasma density) in the summer (northern) hemisphere, while pronounced positive ionospheric storm (increase in plasma density) in the winter (southern) hemisphere. Our observations of decrease of ΔTEC in the Northern Hemisphere and increase of ΔTEC in the Southern Hemisphere do suggest similar results.

Astafyeva et al. (2016) have studied the ionospheric response to this storm using Swarm satellites. Their observations indicated that dayside ionosphere experienced a strong negative ionospheric storm effect from ~22 UT of 22 June to ~1 UT of 23 June, while on the nightside an extreme enhancement of the topside TEC occurred at midlatitudes of the Northern Hemisphere. The EEJ strength variations as obtained from the Swarm data indicates that penetration of storm time electric fields could be the main driver of the observed ionospheric effects in the main phase of the storm. In their observations, the dayside ionosphere first responded to the strong eastward equatorial electric fields and then penetration of westward electric fields led to decrease of the plasma density on the dayside in the topside ionosphere. However, on the nightside, they suggested that extreme enhancement of the Ne and TEC in the Northern Hemisphere in the topside ionosphere are possibly due to the combination of the prompt penetration electric fields, disturbance dynamo and the storm time thermospheric circulation. Our observations of fall and assent of *F* layer height in the midnight period in our observations where we observed strong westward and eastward penetration during nighttime in contrast to their observations.

On 24 June 2015, day under slow recovery phase, we observed sudden increase in the virtual height during pre-sunrise led to spread *F* at Hyderabad and Allahabad. However, we did not observe any spread *F* observations at Tirunelveli, an equatorial station. Since during recovery phase, large chemical and compositional changes occur due to equatorward surge of high-latitude winds/waves, it is possible that they can generate density gradients which are possibly producing observed midlatitude type spread *F*. This type of possibility does exist during summer season where usually equatorial evening Pre-Reversal Enhancement (PRE) is very low. Most of the times, we observe spread *F* in the postmidnight where generation mechanism is still under investigations. While some believe that postmidnight height increase is prerequisite condition, others believe that these are generated in the midlatitudes through *E* region polarization electric fields and might propagate to low latitudes through neutral winds.

In our observations, further, the f_oF_2 shows wave like disturbances between at ~02:30 to 13:30 UT (08:00 19:00 LT) on 23 June during daytime over the all three stations, namely, ALD, HYD, and TIR. The wave-like disturbances possibly associated with TIDs which are generated by the auroral substorm activity. Turunen and Mukunda Rao (1980) reported that the wave-like disturbances in the f_oF_2 associated with the high-velocity traveling atmospheric disturbances (TADs). Lima et al. (2004) suggested that the wave-like disturbances during geomagnetic storms may be associated with the substorm activity when the *AE* index increased. The substorm activity represents the energy injection from the high latitude to low latitudes. Several authors have pointed out that the storm time suppression in the f_oF_2 at midlatitude locations are due to the increase in chemical lose trough by the thermospheric composition changes because of modification in the global thermospheric circulation due to the heating in auroral region (e.g., Matuura, 1972; Prolss, 1977; Rishbeth, 1975; Sastri & Titheridge, 1977). Storm time disturbances affect the occurrence of plasma density and redistribution of ionospheric plasma in the equatorial and low-latitude ionosphere through electric fields, winds/waves, and associated chemical composition change (e.g., Abdu, 1997; Bagiya et al., 2011; Basu et al., 2005; Sastri et al., 2000). During the storm time, separating bottomside and topside ionosphere would be very useful to investigate the ionospheric responses to PPEFs and DDEFs (Kuai et al., 2017). Bagiya et al. (2014) presented in their study over the low latitude that the prompt penetration electric field play an important role for enhancement in global [O/N2] ratio, where the atomic oxygen is directly responsible for the production of the plasma at the *F* region height. They also reported that in their observations, the TEC and f_oF_2 enhanced in the EIA crest region (Northern Hemisphere) at low latitude. The disturbance dynamo during the recovery phase of the magnetic storm has been known to cause the suppression of daytime equatorial ionization anomaly (Sastri, 1988). On 23 June *SYM-H* value reached its minimum value of ~-200 nT at 04:30 UT (10:00 LT). After that the recovery phase started, in the recovery phase all solar wind conditions were constant during 23–24 June. The plasma density variations and composition changes in equatorial ionosphere primarily affected by the *F* region vertical plasma drift, plasma generation, and evolution of plasma structure such as equatorial ionization anomaly (EIA) and ionospheric irregularities (ESF) (e.g., Abdu et al., 1981, 2008; Basu et al., 2005, 2009; Fejer et al., 1999; Mannucci et al., 2005). Significant suppression in f_oF_2 during recovery phase suggest the negative ionospheric storm effect at the low-latitude station at Allahabad and Hyderabad while the positive ionospheric storm effect over the Tirunelveli on 24 June.

The periodogram analysis of IMF B_z, *AE* index, EEJ, and f_oF_2 variations as shown in the Figures 11 and 12 suggests that shorter periods <70 min (in blue circle) are seen in all the parameters indicating that they are driven by PP electric field variations. However, there is no correlation of larger periods of EEJ or f_oF_2 with either IMF B_z or *AE* index. So, accordingly, larger periods of more than 2 h as seen in f_oF_2 are found to be associated with either disturbance winds or DDEFs. It may be recalled that we have seen first peak of the density variation observed at the low-latitude station at Allahabad and after ~1.5 h delay with horizontal phase propagation velocity ~200 m/s reached over the Hyderabad. The similar density variation at the Tirunelveli reached after ~2.5 h delay with phase propagation velocity of ~320 m/s from Hyderabad. Since we see some correlation between one station to other with a time delay, we believe that they could be related to TIDs. However, we do not have any direct evidence to prove that they are related to TIDs.

It is known that EEJ strength undergoes large EEJ/CEJ variations during geomagnetic storms. These variations can be attributed to either the disturbance dynamo electric fields or the overshielding condition. Under overshielding condition, the CEJ is believed to be due to abrupt change in IMF B_z from southward to northward. When the IMF turns northward abruptly, the R1 current abruptly decreases. However, the Region 2 current decreases gradually. This asymmetric change in R1 and R2 currents produce CEJ variations. However, Wei et al. (2009) and Hashimoto et al. (2011) have demonstrated that the overshielding condition can also be achieved after a substorm onset without northward turning of the IMF. The penetration of magnetospheric electric fields to the magnetic equator has been investigated using ground magnetic data along with ionosonde data over Indian sector by Veenadhari et al. (2010). They attributed simultaneous appearance of enhanced DP2 currents and counter electrojets (CEJ) during the main and recovery phases to prompt penetration of electric fields from the high latitudes. Their results suggest that the magnitude of the equatorial ionospheric currents driven by the penetrating electric fields is very much dependent on ionospheric conductivity which again depends on local time. Also, they have seen enhancement of equatorial ionization anomaly (EIA) during the main phase under undersheilding electric fields but reduction of EIA during strong CEJ due to oversheilding electric fields during the recovery phase. On 23 June morning 08:00 IST onward, we see EEJ/CEJ variations even though IMF B_z is steadily in southward direction. Examination of these CEJ variations suggests that they are not linked with IMF B_z. It is possible that the CEJ variations that are not associated with IMF B_z may be associated with Region 2 currents as it is believed that reconfiguration of near-Earth magnetosphere during substorm expansion phase can also generate westward electric fields and CEJ events. However, in one of the CEJ episodes in our case, we have seen simultaneous observation of northward turning of IMF B_z and CEJ event which can be associated with oversheilding electric fields. But in our observations, we do not see any northward turning of IMF B_z after its prolonged southward orientation to cause CEJs over equator. However, we do believe that oversheilding condition might have been achieved through substorm onset to cause multiple CEJ events in the current storm. The *AE* activity also shows that such possibility do exists. On the other hand, disappearance of equatorial *q* type E_s layers over equator during storms is believed to be again due to the imbalance between R1 and R2 currents and has been thoroughly investigated in the past by Rastogi and others. Rastogi (1973) suggested that equatorial *q* type E_s layers disappear simultaneously with the occurrence of DP2 depression in the equatorial geomagnetic fields. They attributed this to temporary reversal of equatorial electric fields from eastward to westward due to DP2 electric fields. In fact, there is a direct linear correlation between equatorial drifts and IMF B_z component (Rastogi & Chandra, 1974). They suggested that sudden reversal of equatorial electric fields have been closely associated with sudden reversal of IMF B_z from southward to northward direction. The presence/absence of the equatorial E_{sq} layers is explained with the help of gradient drift instability. During EEJ currents where both Hall polarization field and density gradients are upward, it is possible to observe E_{sq} layers in the ionograms. However, during CEJ events, when Hall field becomes downward but becomes opposite to density gradient which is upward, it inhibits excitation of gradient drift instability leading to disappearance of equatorial E_{sq}. Based on such results, pervious investigators have suggested that there is a good correlation between storm time CEJ occurrence and absence of equatorial *q* type E_s layers. Our observations of disappearance of equatorial *q* type E_s layers during CEJ events do indicate that E_s layers are indeed affected by the storm time electric field changes. On the other hand, isoheight plots presented here do suggest that *F* layer density variations at shorter periods appears to be associated with EEJ/CEJ variations that are believed to be due to PP electric fields linked with IMF B_z/*AE* activity, while larger periods could be associated with storm time DDEFs or equatorward propagation of high-latitude disturbances such as TIDs.

5. Summary

We studied the electrodynamical changes in the equatorial and low-latitude ionosphere to 2nd major geomagnetic storms (*D*st min ~−200 nT) of the current solar cycle that occurred on 22/23 June 2015 due to double CMEs using chain of ionosondes and GPS receivers over India.

The main findings of the study are as follows:

1. The observations suggest near simultaneous penetration of undershielding and overshielding electric fields during 19:30 UT and 20:30 UT at (local midnight) over Tirunelveli, Hyderabad, and Allahabad on the 22 June 2015 in association with southward/northward IMF B_z fluctuations that caused abrupt decrease of virtual height (*h′F* (km)) to ~200 km due to the strong westward PPEFs and increase to 500 km due to eastward PPEFs near simultaneously over the all three stations.
2. Suppression of spread *F* is observed during westward penetration over Indian sector simultaneously super plasma bubbles were observed in European longitudes where the equatorial type bubbles were detected even at midlatitudes.
3. On 23 June, strong F_3 layers were observed simultaneously at Tirunelveli/Hyderabad in association with IMF B_z which is distinctly different than other days. Further analysis revealed the enhancement of *h′F* (km) at all three ionosonde stations simultaneously at 20:30 UT on 23 June during recovery phase linked to DDEFs.
4. Appearance/disappearance of E_{sq}-type layers at equator during EEJ/CEJ events are linked with storm time electrodynamical changes on 23 June 2015.
5. Our observations of decrease of ΔTEC in the Northern Hemisphere and increase of TEC in the Southern Hemisphere do suggest that our results are similar to model simulations.
6. Interestingly, we noticed early morning spread *F* observations at Hyderabad/Allahabad which is devoid of equatorial spread *F* at Tirunelveli indicates possibility of midlatitude type spread *F* generation at low latitudes possibly generated due to TID propagation.
7. On 24 June, we observed strong negative storm effect over Allahabad/Hyderabad and positive storm effect in Tirunelveli wherein decrease of electron density is observed at Allahabad/Hyderabad and increase of density over Tirunelveli.
8. The oscillatory behavior in the f_oF_2, *h′F* (km), and TEC is noticed during both main and recovery phases. Periodogram analysis of these variations revealed presence of shorter periods (<70 min) and larger periods (>2 h).
9. Based on the our analysis, we suggest that shorter period fluctuations as seen in f_oF_2 are primarily caused by prompt penetration electric field (PPEF) fluctuations, while larger period fluctuations are mainly caused by disturbance winds and TIDs or DDEFs.

Acknowledgments
This work is supported by the in-house project at Indian Institute of Geomagnetism (IIG), Navi Mumbai, India. We are grateful to (a) ACE SWEPAM for providing the IMF B_z data; (b) World Data Centre for Geomagnetism (WDC), Kyoto, for giving *SYM-H*, *AE* (*AU*/*AL*), and *Kp* indices; and (c) GPS TEC data provided by MIT Haystack Observatory Madrigal database. We also would like to thank the Director, IIG, for supporting this research through making available the EEJ strength data. The technical staffs at EGRL/KSKGRL/MO Nagpur are highly acknowledged for their constant support in operating and maintaining the CADI ionosondes and GPS receivers. We thank Buduru Suneel Kumar, in-charge, TIFR Balloon Facility at Hyderabad, for providing Hyderabad CADI ionosonde data. GPS SCINDA data presented here are obtained under joint research work between IIG and AFRL, USA. All the data sets presented in this paper are with S. Sripathi, and he can be contacted through ssripathi.iig@gmail.com.

References

Abdu, M. A. (1997). Major phenomena of the equatorial ionosphere-thermosphere system under disturbed conditions. *Journal of Atmospheric and Solar: Terrestrial Physics*, *59*, 1505–1519.

Abdu, M. A., Bittencourt, J. A., & Batista, I. S. (1981). Magnetic declination control of the equatorial *F* region dynamo electric field development and spread *F*. *Journal of Geophysical Research*, *86*, 11,443–11,446.

Abdu, M. A., de Paula, E. R., Batista, I. S., Reinisch, B. W., Matsuoka, M. T., Camargo, P. O., … de Siqueira, P. M. (2008). Abnormal evening vertical plasma drift and effects on ESF and EIA over Brazil-South Atlantic sector during the 30 October 2003 superstorm. *Journal of Geophysical Research 113*, A07313. https://doi.org/10.1029/2007JA012844

Abdu, M. A., Jayachan, P. T., MacDoug, J., Cecil, J. F., & Sobral, J. H. A. (1998). Equatorial F region zonal plasma irregularity drifts under magnetospheric disturbances. *Geophysical Research Letters*, *25*(22), 4137–4140.

Araki, T., Allen, J. H., & Araki, Y. (1985). Extension of a polar ionospheric current to the night side equator. *Planetary and Space Science*, *33*(1), 11–16.

Astafyeva, E., Zakharenkova, I., & Alken, P. (2016). Prompt penetration electric fields and the extreme topside ionospheric response to the June 22–23, 2015, geomagnetic storms as seen by the Swarm constellation. *Earth, Planets and Space*, *68*, 152. https://doi.org/10.1186/s40623-016-0526

Bagiya, M. S., Hazarika, R., Laskar, F. I., Sunda, S., Gurubaran, S., Chakrabarty, D., … Pallamraju, D. (2014). Effects of prolonged southward interplanetary magnetic field on low-latitude ionospheric electron density. *Journal of Geophysical Research: Space Physics*, *119*, 5764–5776. https://doi.org/10.1002/2014JA020156

Bagiya, M. S., Iyer, K. N., Joshi, H. P., Thampi, S. V., Tsugawa, T., Ravindran, S., … Pathan, B. M. (2011). Low-latitude ionospheric thermospheric response to storm time electrodynamical coupling between high and low latitudes. *Journal of Geophysical Research*, *116*, A01303. https://doi.org/10.1029/2010JA015845

Basu, S., Basu, S., Groves, K. M., Yeh, H.-C., Su, S.-Y., Rich, F. J., … Keskinen, M. J. (2001). Response of the equatorial ionosphere to the great magnetic storm of July 15, 2000. *Geophysical Research Letters*, *28*(18), 3577–3580. https://doi.org/10.1029/2001GL013259

Basu, S., Basu, S., Huba, J., Krall, J., McDonald, S. E., Makela, J. J., … Groves, K. (2009). Day-to-day variability of the equatorial ionization anomaly and scintillations at dusk observed by GUVI and modeling by SAMI3. *Journal of Geophysical Research*, *114*, A04302. https://doi.org/10.1029/2008JA013899

Basu, S., Basu, S., Makela, J. J., Sheehan, R. E., MacKenzie, E., Doherty, P., … Berkey, F. T. (2005). Two components of ionospheric plasma structuring at midlatitudes observed during the large magnetic storm of October 30, 2003. *Geophysical Research Letters*, *32*, L12S06. https://doi.org/10.1029/2004GL021669

Batista, I. S., Abdu, M. A., Souza, J. R., Bertoni, F., Matsuoka, M. T., Camargo, P. O., & Bailey, G. J. (2006). Unusual early morning development of the equatorial anomaly in the Brazilian sector during the Halloween magnetic storm. *Journal of Geophysical Research*, *111*, A05307. https://doi.org/10.1029/2005JA011428

Blanc, M., & Richmond, A. D. (1980). The ionospheric disturbances dynamo. *Journal of Geophysical Research*, *85*, 1669–1686.

Cassak, P. A. (2016). Inside the black box: Magnetic reconnection and the magnetospheric multiscale mission. *Space Weather*, *14*, 186–197. https://doi.org/10.1002/2015SW001313

Cherniak, I., & Zakharenkova, I. (2016). First observations of super plasma bubbles in Europe. *Geophysical Research Letters*, *43*, 11,137–11,145. https://doi.org/10.1002/2016GL071421

Fejer, B. G., de Paula, E. R., Gonzalez, S. A., & Woodman, R. F. (1981). Average vertical and zonal *F* region plasma drifts over Jicamarca. *Journal of Geophysical Research*, *96*(A8), 13,901–13,906. https://doi.org/10.1029/91JA01171

Fejer, B. G., Gonzales, C. A., Farley, D. T., Kelley, M. C., & Woodman, R. F. (1979). Equatorial electric fields during magnetically disturbed conditions: 1. The effect of the interplanetary magnetic field. *Journal of Geophysical Research*, *84*, 5797–5802.

Fejer, B. G., Larsen, M. F., & Farley, D. T. (1983). Equatorial disturbance dynamo electric fields. *Geophysical Research Letters*, *10*(7), 537–540.

Fejer, B. G., Spiro, R. W., Wolf, R. A., & Foster, J. C. (1990). Latitudinal variation of perturbation electric fields during magnetically disturbed periods: 1986 SUNDIAL observations and model results. *Annales de Geophysique*, *8*, 441–454.

Fejer, B. G., de Paula, E. R., Heelis, R. A., & Hanson, W. B. (1995). Global equatorial ionosphere vertical plasma drifts measured by the AE-E satellite. *Journal of Geophysical Research*, *100*, 5769–5776. https://doi.org/10.1029/94JA03240

Fejer, B. G., Scherliess, L., & de Paula, E. R. (1999). Effects of the vertical plasma drift velocity on the generation and evolution of equatorial spread *F*. *Journal of Geophysical Research*, *104*, 19,859–19,869. https://doi.org/10.1029/1999JA900271

Fuller-Rowell, T. J., Codrescu, M. V., Rishbeth, H., Moffett, R. J., & Quegan, S. (1996). On the seasonal response of the thermosphere and ionosphere to geomagnetic storms. *Journal of Geophysical Research*, *101*, 2343–2353.

Gonzales, C. A., Kelley, M. C., & Woodman, R. F. (1979). Equatorial electric fields during magnetically disturbed conditions: Implications of simultaneous auroral and equatorial measurements. *Journal of Geophysical Research*, *84*, 5803–5812.

Hapgood, M. (2017). Satellite navigation Amazing technology but insidious risk: Why everyone needs to understand space weather. *Space Weather*, *15*, 545–548. https://doi.org/10.1002/2017SW001638

Hashimoto, K. K., Kikuchi, T., Watari, S., & Abdu, M. A. (2011). Polarequatorial ionospheric currents driven by the region 2 field-aligned currents at the onset of substorms. *Journal of Geophysical Research*, *116*, A09217. https://doi.org/10.1029/2011JA016442

Heelis, R. A., & Coley, W. R. (2007). Variations in the low and middle latitude topside ion concentration observed by DMSP during superstorm events. *Journal of Geophysical Research*, *112*, A08310. https://doi.org/10.1029/2007JA012326

Huang, C.-S., Foster, J. C., & Kelley, M. C. (2005). Long-duration penetration of the interplanetary electric field to the low-latitude ionosphere during the main phase of magnetic storms. *Journal of Geophysical Research*, *110*, A11309. https://doi.org/10.1029/2005JA011202

Huang, C. S., Sazykin, S., Chau, J. L., Maruyama, N., & Kelley, M. C. (2007). Penetration electric fields: Efficiency and characteristic timescale. *Journal of Atmospheric and Solar-Terrestrial Physics*, *69*, 1135–1146. https://doi.org/10.1016/j.jastp.2006.08.06

Jaggi, R. K., & Wolf, R. A. (1973). Self-consistent calculation of the motion of a sheet of ions in the magnetosphere. *Journal of Geophysical Research*, *78*, 2852–2866. https://doi.org/10.1029/JA078i016p02852

Kamide, Y., Baumjohann, W., Daglis, I. A., Gonzalez, W. D., Grande, M., Joselyn, J. A., … Vasyliunas, V. M. (1998). Current understanding of magnetic storms: Storm-substorm relationships. *Journal of Geophysical Research*, *103*, 17,705–17,728. https://doi.org/10.1029/98JA01426

Kamide, Y., McPherron, R. L., Gonzalez, W. D., Hamilton, D. C., Hudson, H. S., Joselyn, J. A., … Szuszczewicz, E. (1997). Magnetic storms: Current understanding and outstanding questions. In B. T. Tsurutani, et al. (Eds.), *Magnetic Storms* (pp. 1–19). Washington, DC: American Geophysical Union. https://doi.org/10.1029/GM098p0001

Kelly, M. C., Fejer, B. G., & Gonzalez, C. A. (1979). An explanation for anomalous equatorial ionospheric electric fields associated with the northward turning of the interplanetary magnetic field. *Geophysical Research Letters*, *6*(4), 301–304.

Kelley, M. C., Makela, J. J., Chau, J. L., & Nicolls, M. J. (2003). Penetration of the solar wind electric field into the magnetosphere/ionosphere system. *Geophysical Research Letters*, *30*(4), 1158. https://doi.org/10.1029/2002GL016321

Keskinen, M. J., Ossakow, S. L., & Fejer, B. G. (2003). Three-dimensional nonlinear evolution of equatorial ionospheric spread-*F* bubbles. *Geophysical Research Letters*, *30*(16), 1855. https://doi.org/10.1029/2003GL017418

Kikuchi, T. (1986). Evidence of transmission of polar electric fields to the low latitude at times of geomagnetic sudden commencements. *Journal of Geophysical Research*, *91*(A3), 3101–3105.

Kikuchi, T., Hashimoto, K. K., Kitamura, T. I., Tachihara, H., & Fejer, B. (2003). Equatorial counter electrojet during substorms. *Journal of Geophysical Research*, *108*(A11), 1406. https://doi.org/10.1029/2003JA009915

Kikuchi, T., Hashimoto, K. H., & Nazoki, K. (2008). Penetration of magnetospheric electric fields to the equator during a geomagnetic storm. *Journal of Geophysical Research*, *113*, A06214. https://doi.org/10.1029/2007JA012628

Kikuchi, T., Luehr, H., Kitamura, T., Saka, O., & Schlegel, K. (1996). Direct penetration of the polar electric field to the equator during a DP 2 event as detected by the auroral and equatorial magnetometer chains and the EISCAT radar. *Journal of Geophysical Research*, *101*(A8), 17,161–17,173.

Kikuchi, T., Luehr, H., Schlegel, K., Tachihara, H., Shinohara, M., & Kitamura, T.-I. (2000). Penetration of auroral electric fields to the equator during a substorm. *Journal of Geophysical Research*, *105*, 23,251–23,261. https://doi.org/10.1029/2000JA900016

Kil, H., & Paxton, L. J. (2006). Ionospheric disturbances during the magnetic storm of 15 July 2000: Role of the fountain effect and plasma bubbles for the formation of large equatorial plasma density depletions. *Journal of Geophysical Research*, *111*, A12311. https://doi.org/10.1029/2006JA011742

Kuai, J., Liu, L., Lei, J., Liu, J., Zhao, B., Chen, Y., … Hu, L. (2017). Regional differences of the ionospheric response to the July 2012 geomagnetic storm. *Journal of Geophysical Research: Space Physics*, *122*, 4654–4668. https://doi.org/10.1002/2016JA023844

Lee, C. C., Liu, J. Y., Reinisch, B. W., Lee, Y. P., & Liu, L. B. (2002). The propagation of traveling atmospheric disturbances observed during April 6–7, 2000 ionospheric storm in the West Pacific region. *Geophysical Research Letters*, *29*(5), 1068. https://doi.org/10.1029/2001GL013516

Lei, J., Thayer, J. P., Forbes, J. M., Wu, Q., She, C., Wan, W., & Wang, W. (2008). Ionosphere response to solar wind high-speed streams. *Geophysical Research Letters*, *35*, L19105. https://doi.org/10.1029/2008GL035208

Lima, W. L. C., Becker-Guedes, F., Sahai, Y., Fagundes, P. R., Abalde, J. R., Crowley, G., & Bittencourt, J. A. (2004). Response of the equatorial and low-latitude ionosphere during the space weather events of April 2002. *Annales de Geophysique*, *22*, 3211–3219.

Liu, J., Liu, L., Nakamura, T., Zhao, B., Ning, B., & Yoshikawa, A. (2014). A case study of ionospheric storm effects during long-lasting southward IMF B_z-driven geomagnetic storm. *Journal of Geophysical Research: Space Physics*, *19*, 7716–7731. https://doi.org/10.1002/2014JA020273

Mannucci, A. J., Tsurutani, B. T., Iijima, B. A., Komjathy, A., Saito, A., Gonzalez, W. D., … Skoug, R. (2005). Dayside global ionospheric response to the major interplanetary events of October 29–30, 2003 "Halloween storms". *Geophysical Research Letters*, *32*, L12S02. https://doi.org/10.1029/2004GL021467

Matuura, N. (1972). Theoretical models of ionospheric storms. *Space Science Reviews*, *13*, 124–189.

Mikhailov, A. V., & Schlegel, K. (1998). Physical mechanism of strong negative storm effects in the daytime ionospheric F_2 region observed with EISCAT. *Annales de Geophysique*, *16*, 602–608.

Prolss, G. W. (1977). Seasonal variations of atmospheric-ionospheric disturbances. *Journal of Geophysical Research*, *82*, 1635–1640.

Ramsingh, S. S., Sreekumar, S., Banola, S., Emperumal, K., Tiwari, P., & Kumar, B. S. (2015). Low-latitude ionosphere response to super geomagnetic storm of 17/18 March 2015: Results from a chain of ground based observations over Indian sector. *Journal of Geophysical Research: Space Physics*, *120*, 10,864–10,882. https://doi.org/10.1002/2015JA021509

Rastogi, R. G. (1973). E_{sq} layer on Huancayo during March 1970 geomagnetic storm. *Planetary and Space Science*, *21*, 197–203.

Rastogi, R. G., & Chandra, H. (1974). Interplanetary magnetic field and the equatorial ionosphere. *Journal of Atmospheric and Terrestrial Physics*, *36*(2), 377–379.

Rastogi, R. G., & Patel, V. L. (1975). Effect of interplanetary magnetic field on the ionosphere over the magnetic equator. *Proceedings of the Indiana Academy of Sciences*, *82*, 121–141.

Richmond, A. D., & Matsushita, S. (1975). Thermospheric response to a magnetic substorm. *Journal of Geophysical Research*, *80*, 2839–2850.

Rishbeth, H. (1975). *F*-region storms and thermospheric circulation. *Journal of Atmospheric and Terrestrial Physics*, *37*, 1055–1064. https://doi.org/10.1016/0021-9169(75)90013-6

Sastri, J. H. (1988). Equatorial electric-fields of ionospheric disturbance dynamo origin. *Annales de Geophysique*, *6*(6), 635–642.

Sastri, J. H. (1989). Response of equatorial electric field to polarity of inter-planetary magnetic field. *Planetary and Space Science*, *37*, 1403–1408. https://doi.org/10.1016/0032-0633(89)90110-4

Sastri, J. H., Abdu, M. A., Batista, I. S., & Sobral, J. H. A. (1997). Onset conditions of equatorial (range) spread *F* at Fortaleza, Brazil, during the June solstice. *Journal of Geophysical Research*, *102*, 24,013–24,021.

Sastri, J. H., Jyoti, N., Somayajulu, V. V., Chandra, H., & Devasia, C. V. (2000). Ionospheric storm of early November 1993 in the Indian equatorial region. *Journal of Geophysical Research*, *105*, 18,443–18,455. https://doi.org/10.1029/1999JA000372

Sastri, J. H., Niranjan, K., & Subbarao, K. S. V. (2002). Response of the equatorial ionosphere in the Indian (midnight) sector to the severe magnetic storm of July 15, 2000. *Geophysical Research Letters*, *29*(13), 1651. https://doi.org/10.10292002/2002GL015133

Sastri, J. H., Ramesh, K. B., & Karunakaran, D. (1992). On the nature of substorm-related transient electric field disturbances in the equatorial ionosphere. *Planetary and Space Science*, *40*, 95.

Sastri, J. H., & Titheridge, J. E. (1977). Depressions in midlatitude *F*-region under relatively quiet geomagnetic conditions. *Journal of Atmospheric and Solar: Terrestrial Physics*, *39*, 1307–1316.

Somayajulu, V. V. (1998). Magnetosphere-ionosphere coupling. *Proceedings of the Indian National Science Academy*, *64*(A3), 341–351.

Spiro, R. W., Wolf, R. A., & Fejer, B. G. (1988). Penetration of high-latitude-electric-field effects to low latitudes during SUNDIAL 1984. *Annales de Geophysique*, *6*, 39–50.

Tsurutani, B. T., & Gonzalez, W. D. (1997). The interplanetary causes of magnetic storms: A review. In B. T. Tsurutani, et al. (Eds.), *Magnetic Storms* (pp. 77–89). Washington, DC: American Geophysical Union. https://doi.org/10.1029/GM098p0077

Tsurutani, B., Mannucci, A., Iijima, B., Abdu, M. A., Sobral, J. H. A., Gonzalez, W., … Vasyliunas, V. M. (2004). Global dayside ionospheric uplift and enhancement associated with interplanetary electric fields. *Journal of Geophysical Research*, *109*, A08302. https://doi.org/10.1029/2003JA010342

Turunen, T., & Mukunda Rao, M. (1980). Examples of the influence of strong magnetic storms on the equatorial *F*-layer. *Journal of Atmospheric and Terrestrial Physics*, *42*, 323–330.

Veenadhari, B., Alex, S., Kikuchi, T., Shinbori, A., Singh, R., & Chandrasekhar, E. (2010). Penetration of magnetospheric electric fields to the equator and their effects on the low-latitude ionosphere during intense geomagnetic storms. *Journal of Geophysical Research*, *115*, A03305. https://doi.org/10.1029/2009JA014562

Verkhoglyadova, O. P., Tsurutani, B. T., Mannucci, A. J., Mlynczak, M. G., Hunt, L. A., Paxton, L. J., & Komjathy, A. (2016). Solar wind driving of ionosphere-thermosphere responses in three storms near St. Patrick's Day in 2012, 2013, and 2015. *Journal of Geophysical Research: Space Physics*, *121*, 8900–8923. https://doi.org/10.1002/2016JA022883

Wei, Y., Pu, Z., Hong, M., Zong, Q., Ren, Z., Fu, S., … Chu, X. (2009). Westward ionospheric electric field perturbations on the dayside associated with substorm processes. *Journal of Geophysical Research*, *114*, A12209. https://doi.org/10.1029/2009JA014445

Wolf, R. A. (1975). Ionosphere-magnetosphere coupling. *Space Science Reviews*, *17*, 537–562. https://doi.org/10.1007/BF00718584

Zhao, B., Wan, W., Lei, J., Wei, Y., Sahai, Y., & Reinisch, B. (2012). Positive ionospheric storm effects at Latin America longitude during the superstorm of 20–22 November 2003: Revisit. *Annales de Geophysique*, *30*, 831–840.